

The Most Slowly Declining Type Ia Supernova 2001ay

Kevin Krisciunas,¹ Weidong Li,² Thomas Matheson,³ D. Andrew Howell,^{4,5} Maximilian Stritzinger,^{6,7} Greg Aldering,⁸ Perry L. Berlind,⁹ M. Calkins,⁹ Peter Challis,¹⁰ Ryan Chornock,¹⁰ Alexander Conley,¹¹ Alexei V. Filippenko,² Mohan Ganeshalingam,² Lisa Germany,¹² Sergio González,¹³ Samuel D. Gooding,¹ Eric Hsiao,⁸ Daniel Kasen,¹⁴ Robert P. Kirshner,¹⁰ G. H. “Howie” Marion,¹⁰ Cesar Muena,¹³ Peter E. Nugent,⁸ M. Phelps,⁹ Mark M. Phillips,¹³ Yulei Qiu,¹⁵ Robert Quimby,¹⁶ K. Rines,⁹ Jeffrey M. Silverman,² Nicholas B. Suntzeff,¹ Rollin C. Thomas,⁸ and Lifan Wang¹

ABSTRACT

We present optical and near-infrared photometry, as well as ground-based optical spectra and *Hubble Space Telescope* ultraviolet spectra, of the Type Ia supernova (SN) 2001ay. At maximum light the Si II and Mg II lines indicated expansion velocities of 14,000 km s⁻¹, while Si III and S II showed velocities of

¹Department of Physics & Astronomy, George P. and Cynthia Woods Mitchell Institute for Fundamental Physics & Astronomy, Texas A&M University, 4242 TAMU, College Station, TX 77843-4242; krisciunas@physics.tamu.edu, suntzeff@physics.tamu.edu, sam.gooding86@gmail.com, wang@physics.tamu.edu.

²Department of Astronomy, University of California, Berkeley, CA 94720-3411; weidong@astro.berkeley.edu, alex@astro.berkeley.edu, mganesh@astro.berkeley.edu, jsilverman@astro.berkeley.edu.

³National Optical Astronomy Observatories, 950 N. Cherry Avenue, Tucson, AZ 85719-4933; mathe-son@noao.edu.

⁴Las Cumbres Observatory Global Telescope Network, 6740 Cortona Drive, Suite 102, Goleta, CA 93117; ahowell@lcogt.net.

⁵Department of Physics, University of California, Santa Barbara, CA 93106-9530.

⁶The Oskar Klein Centre, Department of Astronomy, Stockholm University, AlbaNova, 10691 Stockholm, Sweden; max.stritzinger@astro.su.se.

⁷Dark Cosmology Centre, Niels Bohr Institute, University of Copenhagen, Juliane Maries Vej 30, 2100 Copenhagen Ø, Denmark; max@dark-cosmology.dk.

⁸Lawrence Berkeley National Laboratory, 1 Cyclotron Road, Berkeley, CA 94720; galdering@lbl.gov, ehsiao@lbl.gov, penugent@lbl.gov, rcthomas@lbl.gov.

⁹Fred L. Whipple Observatory, P. O. Box 97, Amado, AZ 85645; berlind@cfa.harvard.edu.

¹⁰Harvard-Smithsonian Center for Astrophysics, 60 Garden Street, Cambridge, MA 02138; pchal-lis@cfa.harvard.edu, rchornock@cfa.harvard.edu, kirshner@cfa.harvard.edu, hman@astro.as.utexas.edu.

¹¹Department of Astronomy, University of Colorado, Boulder, CO 80309; alexander.conley@colorado.edu.

¹²Swinburne University of Technology, 1 John Street, Hawthorn, VIC, 3122, Australia; lger-many@swin.edu.au.

¹³Las Campanas Observatory, Casilla 601, La Serena, Chile; mmp@lco.cl.

¹⁴Department of Physics, University of California, Berkeley, CA 94720; kasen@berkeley.edu.

¹⁵National Astronomical Observatories of China, Chinese Academy of Sciences, Beijing 100012, China; qiuyi@bao.ac.cn.

¹⁶Department of Astronomy, California Institute of Technology, Pasadena, CA 91125; quimby@astro.caltech.edu.

9,000 km s⁻¹. There is also evidence for some unburned carbon at 12,000 km s⁻¹. SN 2001ay exhibited a decline-rate parameter $\Delta m_{15}(B) = 0.68 \pm 0.05$ mag; this and the *B*-band photometry at $t \gtrsim +25$ d past maximum make it the most slowly declining Type Ia SN yet discovered. Three of four super-Chandrasekhar-mass candidates have decline rates almost as slow as this. After correction for Galactic and host-galaxy extinction, SN 2001ay had $M_B = -19.19$ and $M_V = -19.17$ mag at maximum light; thus, it was *not* overluminous in optical bands. In near-infrared bands it was overluminous only at the 2σ level at most. For a rise time of 18 d (explosion to bolometric maximum) the implied ⁵⁶Ni yield was $(0.58 \pm 0.15)/\alpha M_\odot$, with $\alpha = L_{\text{max}}/E_{\text{Ni}}$ probably in the range 1.0 to 1.2. The ⁵⁶Ni yield is comparable to that of many Type Ia supernovae. The “normal” ⁵⁶Ni yield and the typical peak optical brightness suggest that the very broad optical light curve is explained by the trapping of the γ rays in the inner regions.

Subject headings: supernovae: general — supernovae: individual (SN 2001ay)

1. Introduction

Phillips (1993) first established that Type Ia supernovae (SNe) are *standardizable* candles at optical wavelengths: there is a correlation between their absolute magnitudes at maximum light and the rate at which these objects fade. This fact allowed Type Ia SNe to be used to determine that the expansion of the Universe is currently accelerating (Riess et al. 1998; Perlmutter et al. 1999). More recently, we have discovered that in near-infrared (IR) photometric bands Type Ia SNe are *standard* candles (Meikle 2000; Krisciunas, Phillips, & Suntzeff 2004a; Wood-Vasey, et al. 2008; Folatelli et al. 2010; Mandel, Narayan, & Kirshner 2011). Except for a fraction of the rapidly declining Type Ia SNe whose prototype is SN 1991bg (Filippenko et al. 1992; Leibundgut et al. 1993), which peak in the near-IR after the time of *B*-band maximum, the near-IR absolute magnitudes at maximum light are at most only slightly dependent on the decline-rate parameter $\Delta m_{15}(B)$ (Krisciunas et al. 2009; Folatelli et al. 2010).

We do not understand well how to model a Type Ia SN. For much of the previous decade we thought that (most) Type Ia SNe were carbon-oxygen white dwarfs that approach the Chandrasekhar limit ($1.4 M_\odot$) owing to mass transfer from a nearby companion (for a review, see, e.g., Livio 2000). Some Type Ia SNe might be mergers of two white dwarfs (Iben & Tutukov 1984). Over the past few years the double-degenerate scenario has gained prominence among many researchers. Unfortunately, it is not yet possible to determine with a high degree of probability that a given Type Ia SN is a single or double-degenerate

event, except perhaps for the few that produced more than a Chandrasekhar mass of fusion products; these would result from double-degenerate mergers. An excellent summary of evidence for different kinds of progenitors of Type Ia SNe is given by Howell (2011).

The spectroscopic classification scheme stipulates that Type I SNe do not exhibit obvious hydrogen in their spectra, and that Type II SNe do show prominent hydrogen (Minkowski 1941); see Filippenko (1997) for a review. Type Ia SNe show Si II in absorption, blueshifted from its rest wavelength at 6355 Å. Two objects have been shown to have strong Si II in absorption and H α in emission: SN 2002ic (Hamuy et al. 2003) and SN 2005gj (Aldering et al. 2006; Prieto et al. 2006a). The interpretation is that these objects are Type Ia SNe interacting with circumstellar material (CSM) or (less likely) with the general interstellar medium (ISM).

SN 2006X was found to exhibit variable Na I D absorption (Patat et al. 2007). Two other examples showing variable Na I absorption are SN 1999cl (Blondin et al. 2009) and SN 2006dd (Stritzinger et al. 2010). Light from the SNe is ionizing the circumstellar medium. This leads to recombination and line variations. It should be pointed out that SNe 1999cl and 2006X have large reddening that may involve multiple scattering as well as normal dust extinction (Wang 2005; Goobar 2008).

It is possible to relate the peak bolometric luminosity of a Type Ia SN and the implied amount of radioactive ^{56}Ni produced in the explosion. Most events generate between 0.4 and 0.7 M_{\odot} of ^{56}Ni (Stritzinger et al. 2006). The remarkable SN 2003fg (also known as SNLS-03D3bb; Howell et al. 2006) was sufficiently overluminous that it was regarded to have been caused by the explosion of more than 1.4 M_{\odot} of carbon and oxygen. Three additional super-Chandrasekhar-mass candidates have recently been found: SN 2006gz (Hicken et al. 2007), SN 2007if (Yuan et al. 2010; Scalzo et al. 2010), and SN 2009dc (Yamanaka et al. 2009; Tanaka et al. 2010; Silverman et al. 2010; Taubenberger et al. 2011). As summarized by Scalzo et al. (2010, Table 4), these objects can be up to a magnitude more luminous at optical wavelengths than typical Type Ia SNe. Furthermore, three of these four have extremely slowly declining light curves ($\Delta m_{15}(B) \approx 0.7$ mag). In a double-degenerate system, the more massive white dwarf can tidally disrupt the less massive white dwarf, which has a larger radius. A disk or shell of material is created, retarding the expansion of the more massive white dwarf once it explodes. Another object with a very slow decline rate was SN 2005eq, a target of the Carnegie Supernova Project (Folatelli et al. 2010; Contreras et al. 2010).

In this paper we present optical and near-IR photometry, plus a plethora of spectra, of the equally remarkable SN 2001ay. Preliminary analysis of the light curve and spectra of SN 2001ay is given by Phillips et al. (2003). Two *Hubble Space Telescope* (HST) STIS spectra (from 2001 May 2 and May 9) have already been published by Foley, Filippenko, & Jha

(2008), in a study of possible luminosity indicators in the ultraviolet (UV) spectra of Type Ia SNe.

2. Optical and IR Photometry

SN 2001ay was discovered on 2001 April 18.4 (UT dates are used throughout this paper) by Swift & Li (2001). Its position was $\alpha = 14^{\text{h}}26^{\text{m}}17.0^{\text{s}}$, $\delta = +26^{\circ}14'55.8''$ (J2000), some $10.3''$ west and $9.3''$ north of the nucleus of the spiral galaxy IC 4423. Basic information on SN 2001ay is given in Table 1. Figure 1 shows the host galaxy and SN, and identifies a number of field stars of interest.

A sizable fraction of our optical photometry of SN 2001ay was obtained with the 0.76-m Katzman Automatic Imaging Telescope (KAIT) at Lick Observatory (Li et al. 2000; Filippenko et al. 2001). KAIT images are $6.7' \times 6.7'$ in size, with a scale of $0.80''$ per pixel. For the first three nights of photometry with the Lick Observatory Nickel 1-m telescope, the CCD camera had a chip with $0.30''$ pixels in 2×2 readout mode and gave a field size of $5.1' \times 5.1'$. Thereafter, a new chip was installed, having $0.37''$ pixels in 2×2 readout mode and a field size of $6.3' \times 6.3'$. The two different CCD chips employed with the Nickel telescope had considerably different quantum efficiencies at blue wavelengths.

The *UBVRI* photometry of some field stars near SN 2001ay is found in Table 2. Calibration of optical photometry was accomplished from observations carried out on five photometric nights (two with the CTIO 0.9-m, two with the Nickel, and one with the CTIO 1.5-m telescopes) using the standard stars of Landolt (1992). A subset of our photometry (the KAIT data) has already been published by Ganeshalingam et al. (2010, Table 6), but without K- and S-corrections. Our data presented here were reduced in the IRAF environment.¹⁷ Transformation of the data to the system of Landolt (1992) was accomplished using equations equivalent to those of Wang et al. (2009a). In their Table 1, the reader will find characteristic color terms used for the transformations. Our own direct determinations of these color terms are entirely consistent with their values.

Table 3 gives the J_s and H -band photometry of some of the field stars. We give the averages obtained on seven photometric nights using the Las Campanas 1-m Swope telescope. The calibration was accomplished using a stand-alone version of DAOPHOT, some FORTRAN

¹⁷IRAF is distributed by the National Optical Astronomy Observatory, which is operated by the Association of Universities for Research in Astronomy, Inc., under cooperative agreement with the National Science Foundation (NSF).

programs written by one of us (N.B.S.), and the IR standards of Persson et al. (1998). Thus, our near-IR photometry of SN 2001ay is on the Persson et al. (1998) photometric system.

We can compare the photometry of the principal IR secondary standard (“Star 1”) with data from the Two-Micron All Sky Survey (2MASS; Skrutskie et al. 2006). Whereas we obtained $J_s = 13.718 \pm 0.014$ and $H = 13.251 \pm 0.011$ mag, 2MASS found $J = 13.718 \pm 0.027$ and $H = 13.214 \pm 0.030$ mag. These values are statistically in agreement. For “Star 6” we obtained $J_s = 15.153 \pm 0.021$ and $H = 14.881 \pm 0.008$ mag, whereas 2MASS found $J = 15.132 \pm 0.045$ and $H = 14.807 \pm 0.060$ mag.

Tables 4 and 7 give the optical and IR photometry of SN 2001ay, respectively. Table 4 lists point-spread function (PSF) magnitudes from KAIT, the first three Nickel 1-m nights, and one night of the CTIO 1.5-m telescope; the subtracted template images were obtained with KAIT on 2002 July 9 and 10. For the single night of imaging with the CTIO 1.5-m telescope, the U -band magnitude was determined from aperture photometry; no U -band template was available. For the final night of Nickel 1-m photometry, PSF magnitudes were derived, but without template subtraction. Aperture photometry without template subtraction was conducted for all other optical images.¹⁸

To compare the photometry of different SNe, one should transform the data to the rest-frame equivalent by subtracting the so-called K-corrections (Oke & Sandage 1968; Hamuy et al. 1993; Kim, Goobar, & Perlmutter 1996; Hogg et al. 2002; Nugent, Kim, & Perlmutter 2002). For each SN one computes the time since maximum brightness, and then obtains a rest-frame timescale by dividing the differential times by $1 + z$, where z is the object’s heliocentric redshift. We have worked out the optical K-corrections using actual spectra of SN 2001ay, adopting the Bessell (1990) filter profiles as reference; these are given in Table 5 and shown in Figure 2.

To account for differences in SN photometry that result from the use of different telescopes, CCD chips, and filters, we use the method of spectroscopic corrections (S-corrections), as outlined by Stritzinger et al. (2002) and Krisciunas et al. (2003). For optical bands we adopt as reference the filter specifications of Bessell (1990). *At minimum* one constructs the effective filter profiles using the laboratory transmission curves of the filters multiplied by an appropriate atmospheric function that includes atmospheric absorption lines; then, one multiplies that result by the quantum efficiency of the CCD chip as a function of wavelength. Telescope and instrument optics also contribute to the effective filter

¹⁸Due to the long delay in assembling the data and writing this paper, some images are no longer retrievable from magnetic storage media. Only aperture photometry was possible in 2001, when some of the data were reduced, owing to the lack (at the time) of host-galaxy templates.

profiles. For the KAIT and Nickel 1-m corrections we have used an atmospheric function¹⁹ appropriate to Lick Observatory (elevation 1290 m). For the CTIO 0.9-m data we have used a different atmospheric function appropriate to Cerro Tololo (elevation 2215 m). In practice, one arbitrarily shifts the effective filter profiles toward longer or shorter wavelengths so that synthetic photometry based on spectra of standard stars gives color terms that match those obtained from actual photometry of photometric standards. We used spectra of 50 stars from the sample of Stritzinger et al. (2005) to calculate our synthetic magnitudes using an IRAF script written by one of us (N.B.S.). This script was then used to calculate the S-corrections based on spectra of SN 2001ay itself.

In Figure 3 we show the B - and V -band S-corrections for SN 2001ay. One *adds* these corrections to the photometry. As one can see in Figure 3, if an object like SN 2001ay were observed with the CTIO 0.9-m and Nickel 1-m telescopes, there could be photometric discrepancies as large as ~ 0.06 mag in the B band, depending on the epoch. In the V band the corresponding differences are much smaller.

Even after the application of the S-corrections, we find that the Nickel 1-m B -band data based on aperture magnitudes are systematically 0.09 mag fainter than the KAIT measurements. For the first three nights of Nickel imaging we were able to eliminate these systematic differences by means of template subtraction. The images subsequently obtained with the Nickel 1-m telescope and its newer chip did not lend themselves to image subtraction using the KAIT templates. (Depending on the number of field stars, the angular size of a nearby galaxy in the field, and the seeing, the image rescaling and remapping algorithm can fail.) As a result, we have devised a third set of corrections to the photometry based on images with the new chip in the Nickel camera. Using ADDSTAR within the DAOPHOT package of IRAF, we were able to add an artificial star to the KAIT image-subtraction templates at the pixel location of the SN. This artificial star can be scaled to give a standard magnitude of a desired value such as $B = 17.97$ and $V = 17.14$ mag, just about the brightness of the SN on 2001 May 14 (JD 2,452,043.8), in the middle of the run of Nickel 1-m aperture photometry. Artificial stars having the identical PSF magnitude as the fake star at the location of the SN are placed at blank places in the KAIT templates using ADDSTAR. Since the Nickel 1-m aperture photometry was typically derived with a software aperture of radius 10 pixels (px) and a sky annulus ranging from 12 to 20 px, we can then compare the aperture magnitudes of the fake SN with aperture photometry of the fake stars in the blank places of the image. We use a software aperture radius and sky annulus of identical size in *arc seconds* to that used for the Nickel 1-m photometry. In this way, we can obtain an estimate of the systematic

¹⁹The atmospheric functions combine the mean broad-band extinction values with atmospheric absorption lines.

errors of the SN aperture photometry.

We determined that the B -band magnitudes from Nickel 1-m aperture photometry of the SN were 0.08 mag fainter than what we would have measured without the presence of the host galaxy. Similarly, in the V band we found that the Nickel 1-m aperture magnitudes were fainter by 0.05 mag. For the two nights of CTIO 0.9-m aperture photometry, when the SN was more than 1 mag brighter, the SN was too faint by 0.03 mag in B and V without this correction. Thus, by applying the S-corrections and these additional corrections, we can reconcile almost all systematic differences in the B - and V -band photometry obtained with different telescopes, using different cameras, and using different data-reduction methods (i.e., PSF magnitudes with image-subtraction templates vs. aperture magnitudes without subtractions).

Further justification of this method comes from a consideration of the optical photometry from the first Nickel 1-m chip and the photometry from one night with the CTIO 1.5-m telescope. Data from these four nights *can* be derived using the KAIT host-galaxy templates. In the B band, photometry of the SN using PSF magnitudes and image subtraction was 0.07 to 0.16 mag brighter than aperture photometry using an annulus for the subtraction of the sky level. In the V band, the photometric values of the SN on the first three Nickel 1-m nights were 0.06 mag brighter than values derived from aperture photometry. This result is contrary to typical experience; normally, aperture photometry of a SN is brighter than expected (not fainter) if the SN is located on top of some part of the host galaxy, because the light in the aperture is not entirely due to the SN. That this is not the case here must be due to the relative distributions of host-galaxy light at the SN position and in the sky annulus.

Differences between aperture photometry and PSF photometry are *usually* larger in redder bands. In fact, similar experiments with adding artificial stars to the KAIT templates of SN 2001ay show that the aperture magnitudes with the Nickel 1-m telescope are too bright by 0.01 mag in R and I for the size of the aperture and annulus used. We never obtained near-IR subtraction templates with the camera used on the Las Campanas Observatory 1-m telescope, and that camera has since been decommissioned. So, we must adopt the available near-IR aperture magnitudes.

The I -band photometry is particularly problematic from 15 to 30 d after the time of B -band maximum. Consider the effective filter profiles shown in Figure 4. While the KAIT I -band filter very well approximates the Bessell I filter, the filter used on the Nickel 1-m telescope does not. As the SN achieved its reddest optical colors, a significant excess amount of light is let through by the Nickel 1-m I -band filter. This leads to positive S-corrections; to correct such photometry to Bessell filter photometry requires making the Nickel 1-m

photometry fainter. Our attempts to reconcile up to 0.35 mag differences between the KAIT and Nickel 1-m photometry were not successful. Apparently, the effective filter profile of the Nickel 1-m camera is even more nonstandard than our profile based on laboratory traces of the filter, knowledge of the quantum efficiency as a function of wavelength, and a generic atmospheric function applicable to Lick Observatory. While we list all of our optical photometry in Table 4, the Nickel 1-m *I*-band photometry is not included in our plots or used in the analysis.

The *R*- and *I*-band S-corrections are shown in Figure 5. Note that the photometry in Table 4 includes the K- and S-corrections, plus the corrections mentioned above for CTIO 0.9-m and Nickel 1-m photometry reduced using aperture magnitudes. Since the K-corrected photometry from one night with the YALO 1-m telescope and four nights with the LCO 2.5-m telescope are in good agreement with photometry obtained with other telescopes, and we have no effective transmission curves for the LCO 2.5-m filters used, we have derived no further corrections for this small fraction of our photometry. The interpolated *BVRI* K-corrections and S-corrections are listed in Table 6.²⁰

In spite of the rationale outlined above to reconcile as much of the optical photometry as we can, for a derivation of the maximum brightness and decline rate of SN 2001ay we restrict ourselves to the photometry based on PSF magnitudes with image subtraction. After subtracting the derived K-corrections and adding the S-corrections, we scale the time since maximum light to the rest frame by dividing by $1 + z$. We derive a time of *B*-band maximum of JD 2,452,022.49 ($= 2001$ April 23.0), with an uncertainty of perhaps ± 0.8 d. The decline-rate parameter found from our best *B*-band data is $\Delta m_{15}(B) = 0.68 \pm 0.05$ mag. For comparison, SNe 2005eq had $\Delta m_{15}(B) = 0.72 \pm 0.02$ mag (Folatelli et al. 2010), though Contreras et al. (2010) give $\Delta m_{15}(B) = 0.78 \pm 0.01$ mag. SN 2009dc had $\Delta m_{15}(B) = 0.72 \pm 0.03$ mag (Silverman et al. 2010). SNe 2001ay, 2005eq, 2006gz, 2007if, and 2009dc had extremely slow decline rates. Since it is well established that the energy budget of a Type Ia SN is related to the decline rate, we naturally wonder if SNe 2001ay and 2005eq are also super-Chandrasekhar-mass candidates.

The *B*- and *V*-band light curves of SNe 2001ay, 2005eq, and 2009dc are illustrated in Figure 6. For the first three weeks after maximum light SNe 2001ay and 2009dc were remarkably similar, but at $t \approx 25$ –40 d the light curves diverge. As the peak-to-tail ratio in the *B*- and *V*-band light curves sheds light on the central density and progenitor mass of single-degenerate explosions (Höflich et al. 2010), a comparison of the observational features

²⁰At present, pipelines for SN surveys use template spectra at different epochs since maximum light, warp them, and, adopting appropriate effective filter profiles, calculate the K- and S-corrections at the same time.

and modeling of very slow decliners may yield similar insights.

In Figure 7 we show the unreddened $B - V$ colors of SN 2001ay, the unreddened locus of Lira (1995) and Phillips et al. (1999), and the $\Delta m_{15}(B) = 0.83$ mag locus of Prieto, Rest, & Suntzeff (2006b). On the basis of some of the spectra published here, Branch et al. (2006) classified SN 2001ay as a “broad-line” Type Ia SN. This is the subtype that Wang et al. (2009b) suggest is intrinsically redder than normal Type Ia SNe, or occurs in dustier environments, with $R_V \approx 1.7$. However, Figure 7 shows that, if anything, SN 2001ay is bluer than other normal Type Ia SNe.

In Figure 8 we show the corresponding R - and I -band light curves of SN 2001ay, along with loci derived from the data of SNe 2005eq and 2009dc. The behavior of SN 2001ay in these photometric bands is clearly more like that of SN 2009dc than of SN 2005eq. Note that the I -band secondary maximum of SN 2001ay is essentially as bright as the first maximum.

Figure 9 shows the near-IR photometry of SN 2001ay and the other slow decliners, SNe 2005eq (Folatelli et al. 2010; Contreras et al. 2010) and 2009dc (Stritzinger et al. 2011). SN 1999aw (Strolger et al. 2002) and SN 2001ay were the first objects known to exhibit such flat H -band light curves. (Both H -band light curves are admittedly somewhat ragged, however.) SN 2005eq was the first to show such early near-IR maxima ($t \leq -7$ d). Interestingly, the H -band brightness of SN 2009dc increased steadily over the time frame that the brightness of SN 2001ay was constant.

3. Spectroscopy

We obtained spectra of SN 2001ay on 20 dates using 9 different telescopes; 7 of those nights had spectra with more than one telescope. Spectra were obtained with the 1.5-m telescope of the Fred L. Whipple Observatory (FLWO) on 11 nights. Eight spectra were taken on four nights with the MMT 6.5-m telescope; four with the 2.16-m telescope at the Xinglong Station of the Beijing Astronomical Observatory (BAO); three with the Las Campanas Observatory 2.5-m du Pont telescope; two each with the Lick 3-m Shane reflector (Kast spectrograph) and *HST*; and one each with the Kitt Peak 2.1-m, Kitt Peak 4-m, and Keck II telescopes. The spectroscopic observations with the FLWO 1.5-m and the MMT are summarized in Table 8; we may refer to this as the “CfA set.” A log of other spectroscopic observations is given in Table 9. Some, but not all, of the data were obtained at (or close to) the parallactic angle (Filippenko 1982) in order to minimize the effects of atmospheric dispersion.

In Figure 12 we show a temporal sequence of spectra. Here we have combined the May 2

spectrum from *HST* with the April 29 spectrum from the KPNO 2.1-m telescope. The rather noisy BAO spectra from May 20, 25, and 30 are not illustrated, but the May 10 spectrum from BAO fills a gap in the temporal coverage. We show additional spectra in Figure 13.

Figure 14 includes a portion of our spectrum of SN 2001ay obtained with the Keck Echellette Spectrograph and Imager (ESI; Sheinis et al. 2002) from 2001 April 22 ($t = -1$ d). We find that this maximum-light spectrum exhibits S II and Si III at -9000 km s $^{-1}$. The Si II line (rest wavelength $\lambda_0 = 6355$ Å) and the Mg II line ($\lambda_0 = 4481$ Å) are blueshifted by $14,000$ km s $^{-1}$ at this epoch. There is some gas of these species blueshifted as much as $20,000$ km s $^{-1}$. As shown in Figure 12, by $t = +17$ d the Si II absorption is only blueshifted about $10,000$ km s $^{-1}$.²¹

In our Keck spectrum there is a small absorption dip at an observed wavelength of $\lambda \approx 6520$ Å. If this is due to gas in or near the SN or gas in the ISM of the host galaxy, the wavelength of this line in the frame of the host galaxy is 6315 Å. This may be due to C II ($\lambda_0 = 6580$ Å) blueshifted by $12,000$ km s $^{-1}$. However, other explanations are possible. An absorption feature at 6520 Å in our Galaxy or in the Earth’s atmosphere could lead to a misidentification, given that telluric lines were not removed from the Keck spectrum. One possible such feature is telluric absorption at 6515 Å due to atmospheric water vapor (Matheson et al. 2000, Appendix). We have better evidence of C II absorption in SN 2001ay from the $\lambda_0 = 4745$ Å line, which is seen in the galaxy’s rest frame at 4555 Å, corresponding to an identical blueshift of $12,000$ km s $^{-1}$. We see no evidence of the corresponding C II line with $\lambda_0 = 7234$ Å.

One might expect the C II to be concentrated in the outer layers, and therefore at a higher velocity of approach than sulfur or silicon (Khokhlov, Müller, & Höflich 1993; Gamezo et al. 2003). But if there is mixing or clumpiness, most species could be observed over a broad range of velocities.

In Figure 15 we see the two components of Na I D from gas in the Milky Way and gas in the host galaxy of SN 2001ay. The presence of these lines implies some nonzero amount of reddening and extinction. We find equivalent widths of 0.090 ± 0.018 Å for the Galactic sodium lines and 0.210 ± 0.018 Å for the host-galaxy sodium lines. Using the Munari & Zwitter (1997) calibration of the equivalent width of the sodium lines with $B - V$ color excess, we find $E(B - V)_{\text{Gal}} = 0.026 \pm 0.006$ mag and $E(B - V)_{\text{host}} = 0.072 \pm 0.008$ mag. The Munari & Zwitter (1997) calibration shows a scatter of ± 0.05 mag for $E(B - V)$, which is a more realistic estimate of the uncertainty of the reddening toward SN 2001ay.

²¹For the rest wavelengths of these and other species, see Table 1 of Wang et al. (2006). In their table, however, the rest wavelength of Mg II should read 448.1 nm, not 447.1 nm.

²² The Galactic component may be compared to $E(B - V) = 0.019$ mag obtained by Schlegel, Finkbeiner, & Davis (1998).

In Figure 16 we see the (blueshifted) velocities of Si II $\lambda 4130$ and $\lambda 6355$, with respective error bars of ± 420 and ± 330 km s⁻¹. The $\lambda 6355$ line exhibits the larger velocities because its opacity is greater; we are measuring material farther out in the expanding fireball. The high velocities suggest that the outflow of SN 2001ay is essentially unimpeded, which is consistent with it having been a single-degenerate explosion; however, Maeda et al. (2010) emphasize the importance of the viewing angle on the observed properties of Type Ia SNe. We cannot state with certainty whether SN 2001ay was a single or double-degenerate explosion.

The $\lambda 4130$ line gives a velocity gradient of $\dot{v} = 226 \pm 32$ km s⁻¹ d⁻¹, while the $\lambda 6355$ line gives $\dot{v} = 171 \pm 35$ km s⁻¹ d⁻¹. The Si II velocity gradient is considerably higher than 70 km s⁻¹ d⁻¹, the criterion of Benetti et al. (2005) to include SN 2001ay with other “high velocity gradient” Type Ia SNe.

4. Discussion

4.1. Reddening

As mentioned above, the Galactic reddening along the line of sight to SN 2001ay is $E(B - V) = 0.026$ mag, and the host-galaxy component is $E(B - V) = 0.072$ mag. Thus, for SN 2001ay, $E(B - V)_{\text{total}} \approx 0.098$ mag. Normal Galactic dust is characterized by an average value of $R_V = A_V/E(B - V) = 3.1$ (Cardelli, Clayton, & Mathis 1989), but dust associated with Type Ia SNe is often characterized by a lower value; see, for example, Krisciunas et al. (2007). If we adopt $R_V = 3.1$ for the Galactic component of reddening for SN 2001ay and $R_V = 2.4 \pm 0.2$ for the host-galaxy reddening, it follows that $A_B = 0.35 \pm 0.08$, $A_V = 0.25 \pm 0.06$, $A_R = 0.21 \pm 0.05$, $A_I = 0.15 \pm 0.04$, $A_J = 0.08 \pm 0.02$, and $A_H = 0.04 \pm 0.01$ mag (Krisciunas et al. 2006, Table 8).

4.2. Absolute Magnitudes at Maximum Light

Garnavich et al. (2004) give BVI decline-rate relations for what was then the known range of $\Delta m_{15}(B)$ for Type Ia SNe. The slowest decliner used by Prieto, Rest, & Suntzeff

²²However, Poznanski et al. (2011) recently found that the uncertainty of the reddening derived from the Na I D lines may be substantially larger than this.

(2006b) for their light-curve fitting template algorithm was SN 1999aa, with $\Delta m_{15}(B) = 0.83$ mag. For such a decline-rate parameter, the implied absolute magnitudes at maximum are $M_B = -19.42$, $M_V = -19.39$, and $M_I = -18.85$ on an $H_0 = 72 \text{ km s}^{-1} \text{ Mpc}^{-1}$ distance scale. Three of the four super-Chandrasekhar-mass Type Ia SN candidates discussed by Scalzo et al. (2010) are significantly more luminous than this.

In Figure 10 we show the absolute V -band magnitudes at maximum light of SNe 2001ay, 2003fg, 2005eq, 2006gz, 2007if, and 2009dc, along with the V -band decline-rate relation of Garnavich et al. (2004). Figure 11 gives the near-IR absolute magnitudes of Type Ia SNe at their respective maxima, including SNe 2001ay and 2005eq. Three of the four super-Chandra candidates are overluminous, while all other very slow decliners have “normal” maximum brightness.

Based on our best optical photometry (using PSF magnitudes and image-subtraction templates), we find apparent magnitudes for SN 2001ay of $B_{\text{max}} = 16.71$, $V_{\text{max}} = 16.64$, $R_{\text{max}} = 16.65$, and $I_{\text{max}} = 16.79$. These values include the K -corrections and S -corrections. Given the extinction values listed above and the distance modulus of the host galaxy given in Table 1, at maximum light we find $M_B = -19.19 \pm 0.12$, $M_V = -19.17$, $M_R = -19.10$, and $M_I = -18.90$ mag (with uncertainties of ± 0.10 mag); thus, SN 2001ay was *not* overluminous at optical wavelengths.

Typically, Type Ia SNe peak in the near-IR ~ 3 d prior to the time of B -band maximum (Krisciunas et al. 2004b). SN 2005eq peaked at least 7 d prior to B maximum. We surmise that SN 2001ay may have been ~ 0.12 mag brighter at maximum light than our first J_s measurement, or $J_s(\text{max}) \approx 16.85$ mag. In the H band SN 2001ay exhibited a very flat light curve; we adopt $H_{\text{max}} = 16.97 \pm 0.08$ mag. The corresponding extinction-corrected absolute magnitudes at IR maximum are $M_{J_s} = -18.77 \pm 0.10$ and $M_H = -18.62 \pm 0.10$. These values may be compared to the mean values of all but the late-peaking fast decliners from Krisciunas et al. (2009), namely $\langle M_J \rangle = -18.61$ and $\langle M_H \rangle = -18.31$ mag. The standard deviations of the distributions of the near-IR absolute magnitudes are about ± 0.15 mag. In the J_s and H bands, SN 2001ay was overluminous by $\sim 1\sigma$ and 2σ , respectively; hence, SN 2001ay was not statistically significantly brighter in the near-IR than other Type Ia SNe.

4.3. Bolometric Light Curve and Mass Budget

In Figure 17 we show the bolometric light curve of SN 2001ay, based on our broad-band photometry. Though Type Ia SNe near maximum light have spectral energy distributions that peak at optical wavelengths, they also emit UV and IR light. One might scale the

integrated flux by a factor of ~ 1.1 to account for UV and IR light not included in the optical bandpasses (Stritzinger et al. 2006), but according to Blinnikov et al. (2006) this still underestimates the bolometric flux. Adopting distance modulus 35.55 mag ($D \approx 129$ Mpc; see Table 1) and a scale factor of 1.15, we obtain a peak derived bolometric luminosity ($4\pi D^2$ times the bolometric flux) of 1.20×10^{43} erg s $^{-1}$. Figure 17 also shows the bolometric light curves of SNe 2007if and 2009dc.

At maximum light the luminosity produced by radioactive ^{56}Ni is given by

$$L_{\text{max}} = \alpha E_{\text{Ni}} , \quad (1)$$

where E_{Ni} is the energy input from the decay of ^{56}Ni , evaluated at the time of bolometric maximum. Arnett’s Rule implies that $\alpha = 1$ (Arnett 1982), meaning that the gamma-ray deposition matches the bolometric flux at maximum light. However, the value of α can actually range from 0.8 to 1.3, depending on the explosion model. For a delayed detonation model $\alpha = 1.2$ is appropriate (Khokhlov, Müller, & Höflich 1993, Fig. 36); see also Höflich & Khokhlov (1996). Howell et al. (2006) adopt $\alpha = 1.2$.

In Figure 18 we show the radioactive decay energy deposition function fit to the last few points of the bolometric light curve. In this figure we also show the cases of complete trapping of the γ rays and complete γ -ray escape. We adopt a rise time of 18 d from explosion to bolometric maximum, comparable to observational results of Garg et al. (2007) for other Type Ia SNe. Hayden et al. (2010) find an average rise time in the B band of 17.38 d, with a range of 13 to 23 d, while the B -band rise time determined by Ganeshalingam, Li, & Filippenko (2011) is about 18 d. Figure 18 uses $\alpha = 1.0$.²³

The energy deposited by 1 M_{\odot} of ^{56}Ni into the explosion of a Type Ia SN is given by Stritzinger & Leibundgut (2005) as

$$E_{\text{Ni}}(1 M_{\odot}) = (6.45 \times 10^{43})e^{-t_R/8.8} + (1.45 \times 10^{43})e^{-t_R/111.3} , \quad (2)$$

where t_R is the rise time in days from the moment of explosion to the time of bolometric maximum. The e -folding times of ^{56}Ni and ^{56}Co are 8.8 and 111.3 d, respectively. For $t_R = 18$ d and $\alpha = 1.0$, $L_{\text{max}} = 2.07 \times 10^{43}$ erg s $^{-1}$ M_{\odot}^{-1} ; for $\alpha = 1.2$, $L_{\text{max}} = 2.48 \times 10^{43}$ erg s $^{-1}$ M_{\odot}^{-1} .

²³The writers of this section could not come to a consensus on the best value of α to adopt, so in what follows we give the results for $\alpha = 1.0$ and 1.2. Baron et al. (2011) choose $\alpha = 0.9$ for their SN 2001ay model.

There was a nondetection of SN 2001ay on April 5.4,²⁴ which was 17.1 rest-frame days before the time of B -band maximum. The upper limit of the brightness on that date was $R \approx 19.5$ mag, or ~ 3 mag fainter than the observed R -band maximum. Although we have an image of the host galaxy at $t = -17$ d, we would need to reach a much fainter magnitude limit to place a useful constraint on the time of the explosion. The lack of premaximum photometry does not allow us to determine the rise time of SN 2001ay.

To obtain the ^{56}Ni yield in solar masses, we simply divide the peak luminosity (1.20×10^{43} erg s $^{-1}$) by the coefficient given above for the adopted rise time (e.g., $2.07 \times 10^{43} \times \alpha$ for $t_R = 18$ d); the result is $0.58/\alpha$ M_\odot of ^{56}Ni . SN 2001ay certainly did not produce more than a Chandrasekhar mass of ^{56}Ni .

A 5% uncertainty in the value of H_0 leads to a 10% uncertainty in the luminosity calculated from the optical photometry. Given the uncertainties in the parameter α in Equation 1 and uncertainty in the adopted bolometric rise time, the minimum uncertainty in the ^{56}Ni yield is about ± 0.15 M_\odot divided by α .

We would like to estimate the mass in the ejecta of SN 2001ay. Following Jeffrey (1999) and Stritzinger et al. (2006), the “fiducial time” (t_0) is the time scale for the ejecta to become optically thin:

$$t_0 = \left(\frac{M_{\text{ej}} \kappa q}{8\pi} \right)^{\frac{1}{2}} \frac{1}{v_e}, \quad (3)$$

where M_{ej} is the ejecta mass, κ is the γ -ray mean opacity, q is a dimensionless scale factor, and v_e is the e -folding velocity of an exponential model’s density profile. Stritzinger et al. (2006) adopt $\kappa = 0.025$ cm 2 g $^{-1}$ and $v_e = 3000$ km s $^{-1}$. They also choose $q = 1/3$, meaning that ^{56}Ni was distributed throughout the ejecta; $q = 1$ for high concentrations of ^{56}Ni at the center of the ejecta. Using the last three points in our bolometric light curve (from $t = 49$ to 111 d), adopting $\alpha = 1.2$, and using a ^{56}Ni yield of 0.48 M_\odot we derive a “fiducial time” of 66.2 ± 3.0 d. Taking $\alpha = 1.0$ and a ^{56}Ni yield of 0.58 M_\odot gives $t_0 = 57.2 \pm 2.4$ d. Both of these values are considerably longer than the 22 d to 35 d in Table 1 of Stritzinger et al. (2006), but not much greater than the 51 d for SN 2007if given in Figure 9 of Scalzo et al. (2010). The SN 2001ay fiducial time depends critically on the final point in the bolometric light curve, a point derived from PSF photometry without template subtraction (hence possibly erroneous). Using $t_0 = 66.2$ d and the values of q , v_e , and κ adopted by Stritzinger et al. (2006), the implied ejecta mass is 4.4 M_\odot , which is clearly wrong. For $t_0 = 57.2$ d and the

²⁴Swift & Li (2001) incorrectly give the date of this nondetection as 2001 April 4.4.

higher ^{56}Ni yield, the implied ejecta mass is $3.3 M_{\odot}$. Adopting $q = 1$ instead could cut these down by a factor of three. Choosing $q = 1/3$ but $v_e = 1500 \text{ km s}^{-1}$ would give 0.8 to $1.1 M_{\odot}$ for the ejecta mass. The lower e -folding velocity is only slightly less than what one derives from the three-dimensional models of Röpke & Hillebrandt (2004). Given the uncertainties of the parameters necessary for Eq. 3 and the lack of high-quality photometry from ~ 50 to 100 d after maximum light, we feel that a robust calculation of the ejecta mass of SN 2001ay is beyond the scope of this paper.

We note that Taubenberger et al. (2011) derived an ejecta mass for SN 2009dc of $2.8 M_{\odot}$, based on the expansion velocity and the timescale around maximum brightness, which depends on the optical opacity. They describe their result as “an utmost challenge for all scenarios that invoke thermonuclear explosions of white dwarfs.”

4.4. Spectroscopic Comparison and Modeling

Wagers, Wang, & Asztalos (2010) have used wavelet analysis to search for spectroscopic correlations of Type Ia SNe. Their results are based on the analysis of a few dozen relatively nearby objects ($z \lesssim 0.04$). SN 2001ay is anomalous in a number of their plots, particularly their Figure 12, showing the correlation of the strength of the 4570 \AA emission feature vs. $\Delta m_{15}(B)$.

In Figure 19 we illustrate a comparison of the spectra of SNe 2001ay, 2005eq, and 2009dc. The most obvious difference between SN 2001ay and these other two objects is the much larger blueshift of Si II seen in SN 2001ay prior to B maximum. Also, the C II absorption in SN 2009dc is much stronger. SN 2005eq was apparently the hottest of the three, given the stronger presence of doubly ionized iron and the weakness of singly ionized species. This is more like the classical slow decliner SN 1991T (Filippenko 1997), which is, in fact, how Contreras et al. (2010, Table 1) classify SN 2005eq.

In Table 10 we give a summary of some observational characteristics of SNe 2001ay, 2005eq, and 2009dc. Given the divergence of the light curves of SN 2005eq seen in Figure 6 compared to the other two objects, the larger decline-rate parameter of SN 2005eq ($\Delta m_{15}(B) = 0.78 \text{ mag}$) from Contreras et al. (2010) is more likely correct than the value of $\Delta m_{15}(B) = 0.72 \text{ mag}$ from Folatelli et al. (2010), though we have used the latter to plot SN 2005eq in Figure 10. SNe 2001ay and 2009dc have almost the same optical decline rate. SN 2001ay had normal optical peak brightness and high Si II velocity. SN 2009dc was overluminous at optical maximum and had much lower Si II velocity. Their H -band light curves are unlike those of any other Type Ia SNe observed thus far, except for SN 1999aw.

To investigate the details of our SN spectra, we use the SN spectrum-synthesis code SYNOW (Fisher et al. 1997). Although SYNOW has a simple, parametric approach to creating synthetic spectra, it is a powerful tool to aid line identifications which in turn provide insights into the spectral formation of the objects. To generate a synthetic spectrum one inputs a blackbody temperature (T_{BB}), a photospheric velocity (v_{ph}), and for each involved ion, an optical depth at a reference line, an excitation temperature (T_{exc}), and the maximum velocity of the opacity distribution (v_{max}). Moreover, it assumes that the optical depth declines exponentially for velocities above v_{ph} with an e -folding scale of v_e . The strengths of the lines for each ion are determined by oscillator strengths, and the approximation of a Boltzmann distribution of the lower level populations is set by the temperature T_{exc} .

In Figure 20, we present our -1 d spectrum of SN 2001ay with a synthetic spectrum generated from SYNOW. This fit has $T_{\text{BB}} = 20,500$ K and $v_{\text{ph}} = 12,000$ km s $^{-1}$. The majority of the observed features are well fit by the synthetic spectrum. The ions used in the fit, as labeled in the figure, are commonly observed in the near-maximum spectra of Type Ia SNe (Branch et al. 2005) with the exception of C II. Although the inclusion of C II in the fit produces an absorption feature at ~ 6300 Å (due to C II $\lambda 6580$) that is too strong compared to the observed spectrum, it nonetheless yields a better fit to the absorption feature at ~ 4500 Å (due to C II $\lambda 4745$), so we conclude that the inclusion of C II marginally improves the SYNOW fit.

We attempt SYNOW fits to the SN 2001ay spectra at $t \approx +6$ d and 23 d. Figure 21 shows the result for the $t \approx +6$ d spectrum. The model spectrum has $T_{\text{BB}} = 14,000$ K and $v_{\text{ph}} = 11,000$ km s $^{-1}$, and has all the regular ions observed in a Type Ia SN. C II is no longer needed, but a relatively strong Na I line is now observed at ~ 5600 Å. A SYNOW fit for the $t \approx 23$ d spectrum (not shown) requires $T_{\text{BB}} = 8500$ K and $v_{\text{ph}} = 9000$ km s $^{-1}$.

Finally, in Figure 22 we show a model fit to our Keck spectrum using the SYNAPPS code of Thomas et al. (2011). The physical assumptions SYNAPPS uses match those of SYNOW (Fisher et al. 1997), so findings are restricted to identification of features and not quantitative abundances. But where SYNOW is completely interactive, SYNAPPS is automated. This relieves the user from iterative adjustment of a large number of parameters (over 50 variables) to gain fit agreement and assures more exhaustive searching of the parameter space. SYNAPPS can be thought of as the hybridization of a SYNOW-like calculation with a parallel optimization framework, where spectral fit quality serves as the objective function to optimize. A good fit constrains explosion models through interpretive spectral feature identification, with the main result being the detection or exclusion of specific chemical elements. The velocity distribution of detected species within the ejecta can also be constrained.

SYNAPPS indicates that SN 2001ay had a photospheric velocity of 10,800 km s $^{-1}$ at

$t = -1$ d, which should be robust, as it is derived from 11 ions, namely C II, O I, Mg II, Si II, Si III, S II, Ca II, Fe II, Fe III, Co II, and Ni II. We are confident of the presence of C II.

5. Conclusions

We have presented the available spectra, as well as optical and near-IR photometry, of SN 2001ay.

While SN 2001ay is the most slowly declining Type Ia SN ever discovered, it was not overluminous in optical bandpasses. In near-IR bands it was overluminous only at the 2σ level at most. Unlike other very slow decliners such as SNe 2003fg, 2007if, and 2009dc, which were significantly overluminous, we do not have any evidence that SN 2001ay was a super-Chandrasekhar-mass explosion.

SN 2001ay showed evidence for C II, but it was much weaker than in SN 2009dc. At early times Mg II and Si II were observed in SN 2001ay at high velocity (14,000 km s⁻¹ and higher). By contrast, spectra of SN 2009dc did not show large velocities for Mg II and Si II. On the basis of a small number of super-Chandrasekhar-mass candidates, it seems that these objects exhibit rather low velocities, possibly the result of retardation due to a shell of material arising from the disruption of the less massive white dwarf in a double-degenerate system.

SN 2001ay produced $(0.58 \pm 0.15)/\alpha$ M_⊙ of ⁵⁶Ni, considerably less than a Chandrasekhar mass. The value of α probably lies in the range 1.0 to 1.2. Naively, one might conclude that SN 2001ay was a single-degenerate explosion, but this is hardly a firm conclusion. The very broad light curve might be explained by the trapping of the γ rays in the explosion. An explanation of the extremely slow decline will be discussed in a subsequent paper (Baron et al. 2011).

The work presented here is based in part on observations made with the NASA/ESA *Hubble Space Telescope*, obtained at the Space Telescope Science Institute, which is operated by the Association of Universities for Research in Astronomy, Inc., under NASA contract NAS5-26555; the Cerro Tololo Inter-American Observatory and the Kitt Peak National Observatory of the National Optical Astronomy Observatory, which is operated by the Association of Universities for Research in Astronomy, Inc. (AURA) under cooperative agreement with the NSF; the MMT Observatory, a joint facility of the Smithsonian Institution and the University of Arizona; the Fred L. Whipple Observatory; the Lick Observatory

of the University of California; the Las Campanas Observatory; the Beijing Astronomical Observatory; and the W. M. Keck Observatory, which was generously funded by the W. M. Keck Foundation and is operated as a scientific partnership among the California Institute of Technology, the University of California, and NASA. We thank the staffs at these observatories for their efficient assistance, Don Groom for taking some of the Nickel 1-m images, and Rachel Gibbons, Maryam Modjaz, Isobel Hook, and Saul Perlmutter for other observational assistance. We are grateful to Peter Höflich, Alexei Khokhlov, and Eddie Baron for comments on §4.3.

The supernova research of A.V.F.’s group at U. C. Berkeley is supported by NSF grant AST-0908886 and by the TABASGO Foundation, as well as by NASA through grants AR-11248 and AR-12126 from the Space Telescope Science Institute, which is operated by Associated Universities for Research in Astronomy, Inc., under NASA contract NAS 5-26555. KAIT and its ongoing operation were made possible by donations from Sun Microsystems, Inc., the Hewlett-Packard Company, AutoScope Corporation, Lick Observatory, the NSF, the University of California, the Sylvia & Jim Katzman Foundation, and the TABASGO Foundation. J.M.S. is grateful to Marc J. Staley for a Graduate Fellowship. K. K., L. W., and N. B. S. are supported in part by NSF grant AST-0709181. Supernova research at Harvard is supported by NSF grant AST-0907903. This work was also supported by the Director, Office of Science, Office of High Energy Physics, of the U.S. Department of Energy under Contract No. DE-AC02-05CH11231.

REFERENCES

- Aldering, G., et al. 2006, *ApJ*, 650, 510
- Arnett, W. D. 1982, *ApJ*, 253, 785
- Baron, E., et al. 2011, in preparation
- Beers, T. C., Kriessler, J. R., Bird, C. M., & Huchra, J. P. 1995, *AJ*, 109, 874
- Benetti, S., et al. 2005, *ApJ*, 623, 1011
- Bessell, M. S. 1990, *PASP*, 102, 1181
- Blinnikov, S. I., Röpke, F. K., Sorokina, E. I., Gieseler, M., Reinecke, M., Travaglio, C., Hillebrandt, W., & Stritzinger, M. 2006, *A&A*, 453, 229
- Blondin, S., Prieto, J. L., Patat, F., Challis, P., Hicken, M., Kirshner, R. P., Matheson, T., & Modjaz, M. 2009, *ApJ*, 693, 207

- Branch, D., Baron, E., Hall, N., Melakayil, M., & Parrent, J. 2005, *PASP*, 117, 545
- Branch, D., et al. 2006, *PASP*, 118, 560
- Cardelli, J. A., Clayton, G. C., & Mathis, J. S. 1989, *ApJ*, 345, 245
- Contreras, C., et al. 2010, *AJ*, 139, 519
- Filippenko, A. V. 1982, *PASP*, 94, 715
- Filippenko, A. V. 1997, *ARA&A*, 35, 309
- Filippenko A. V., Li W., Treffers R. R., & Modjaz M. 2001, in *Small-Telescope Astronomy on Global Scales*, ed. W. P. Chen, C. Lemme, & B. Paczyński (San Francisco: ASP), 121
- Filippenko, A. V., et al. 1992, *AJ*, 104, 1543
- Fisher, A., Branch, D., Nugent, P., & Baron, E. 1997, *ApJ*, 481, L89
- Folatelli, G., et al. 2010, *AJ*, 139, 120
- Foley, R., Filippenko, A. V., & Jha, S. W. 2008, *ApJ*, 686, 117
- Freedman, W., et al. 2001, *ApJ*, 553, 47
- Gamezo, V. N., Khokhlov, A. M., Oran, E. S., Chtchelkanova, A. Y., & Rosenberg, R. O. 2003, *Science*, 299, 77
- Ganeshalingam, M., et al. 2010, *ApJS*, 190, 418
- Ganeshalingam, M., Li, W., & Filippenko, A. V. 2011, *MNRAS*, in press
- Garg, A., et al. 2007, *AJ*, 133, 403
- Garnavich, P., et al. 2004, *ApJ*, 613, 1120
- Goobar, A. 2008, *ApJ*, 686, 103
- Hamuy, M., Phillips, M. M., Wells, L. A., & Maza, J. 1993, *PASP*, 105, 787
- Hamuy, M., et al. 2003, *Nature*, 424, 651
- Hayden, B. T., et al. 2010, *ApJ*, 712, 350
- Hicken, M., et al. 2007, *ApJ*, 669, L17

- Höflich, P., & Khokhlov, A. 1996, *ApJ*, 457, 500
- Höflich, P., et al. 2010, *ApJ*, 710, 444
- Hogg, D. W., Baldry, I. K., Blanton, M. R., & Eisenstein, D. J. 2002 (arXiv:astro-ph/0210394)
- Howell, D. A., et al. 2006, *Nature*, 443, 308
- Howell, D. A. 2011, *Nature Commun.*, in press (arXiv:1011.0441)
- Iben, I., Jr., & Tutukov, A. V. 1984, *ApJS*, 54, 335
- Jeffrey, D. J. 1999 (arXiv:astro-ph/9907015)
- Khokhlov, A., Müller, E., & Höflich, P. 1993, *A&A*, 270, 223
- Kim, A., Goobar, A., & Perlmutter, S. 1996, *PASP*, 108, 190
- Krisciunas, K., Phillips, M. M., & Suntzeff, N. B. 2004a, *ApJ*, 602, L81
- Krisciunas, K., Prieto, J. L., Garnavich, P. M., Riley, J.-L. G., Rest, A., Stubbs, C., & McMillan, R. 2006, *AJ*, 131, 1639
- Krisciunas, K., et al. 2003, *AJ*, 125, 166
- Krisciunas, K., et al. 2004b, *AJ*, 128, 3034
- Krisciunas, K., et al. 2007, *AJ*, 133, 58
- Krisciunas, K., et al. 2009, *AJ*, 138, 1584
- Landolt, A. U. 1992, *AJ*, 104, 340
- Leibundgut, B., et al. 1993, *AJ*, 105, 301
- Li, W., et al. 2000, in *Cosmic Explosions*, ed. S. S. Holt & W. W. Zhang (New York: AIP), 103
- Lira, P. 1995, Master's Thesis, Univ. Chile
- Livio, M. 2000, in *The Greatest Explosions since the Big Bang: Supernovae and Gamma-Ray Bursts*, ed. M. Livio, N. Panagia, & K. Sahu (Baltimore: STScI), 334
- Maeda, K., et al. 2010, *Nature*, 466, 82

- Mandel, K. S., Narayan, G., & Kirshner, R. P. 2011, *ApJ*, in press (arXiv:1011.5910)
- Matheson, T., Filippenko, A. V., Ho, L. C., Barth, A. J., & Leonard, D. C. 2000, *AJ*, 120, 1499
- Meikle, W. P. S. 2000, *MNRAS*, 314, 782
- Minkowski, R. 1941, *PASP*, 53, 224
- Munari, U., & Zwitter, T. 1997, *A&A*, 318, 269
- Nugent, P., Kim, A., & Perlmutter, S. 2002, *PASP*, 114, 803
- Oke, J. B., & Sandage, A., 1968, *ApJ*, 154, 21
- Patat, F., et al. 2007, *Science*, 317, 924
- Perlmutter, S., et al. 1999, *ApJ*, 517, 565
- Persson, S. E., Murphy, D. C., Krzeminski, W., Roth, M., & Rieke, M. J. 1998, *AJ*, 116, 2475
- Phillips, M. M. 1993, *ApJ*, 413, L105
- Phillips, M. M., Lira, P., Suntzeff, N. B., Schommer, R. A., Hamuy, M., & Maza, J. 1999, *AJ*, 118, 1766
- Phillips, M. M., et al. 2003, in *From Twilight to Highlight*, ed. W. Hillebrandt, B. Leibundgut (Berlin: Springer-Verlag), 193
- Poznanski, D., Ganeshalingam, M., Silverman, J. M., & Filippenko, A. V. 2011, *MNRAS*, in press
- Prieto, J. L., et al. 2006a (arXiv:0706.4088)
- Prieto, J. L., Rest, A., & Suntzeff, N. B. 2006b, *ApJ*, 647, 501
- Riess, A. G., et al. 1998, *AJ*, 116, 1009
- Riess, A. G., et al. 2009, *ApJ*, 699, 539
- Röpke, F. K., & Hillebrandt, W. 2004, *A&A*, 420, L1
- Scalzo, R. A., et al. 2010, *ApJ*, 713, 1073
- Schlegel, D. J., Finkbeiner, D. P., & Davis, M. 1998, *ApJ*, 500, 525

- Sheinis, A. I., Bolte, M., Epps, H. W., Kibrick, R. I., Miller, J. S., Radovan, M. V., Bigelow, B. C., & Sutin, B. M., 2002, *PASP*, 114, 851
- Silverman, J. M., Ganeshalingam, M., Li, W. D., Filippenko, A. V., Miller, A. A., & Poznanski, D. 2010, *MNRAS*, 410, 585
- Skrutskie, M. F., et al. 2006, *AJ*, 131, 1163
- Stritzinger, M., et al. 2002, *AJ*, 124, 2100
- Stritzinger, M., & Leibundgut, B. 2005, *A&A*, 431, 423
- Stritzinger, M., Suntzeff, N. B., Hamuy, M., Challis, P., Demarco, R., Germany, L., & Soderberg, A. M. 2005, *PASP*, 117 810
- Stritzinger, M., Leibundgut, B., Walch, S., & Contardo, G. 2006, *A&A*, 450, 241
- Stritzinger, M., et al. 2010, *AJ*, 140, 2036
- Stritzinger, M., et al. 2011, in press
- Strolger, L.-G., et al. 2002, *AJ*, 124, 2905
- Swift, B., & Li, W. D. 2001, *IAU Circ.* 7611
- Tanaka, M., et al. 2010, *ApJ*, 714, 1209
- Taubenberger, S., et al. 2011, *MNRAS*, in press (arXiv:1011.5665)
- Thomas, R., et al. 2011, *PASP*, in press
- Wagers, A., Wang, L., & Asztalos, S. 2010, *ApJ*, 711, 711
- Wang, L. 2005, *ApJ*, 635, L33
- Wang, L., Baade, D., Höflich, P., Wheeler, J. C., Kawabata, K., Khokhlov, A., Nomoto, K., & Patat, F. 2006, *ApJ*, 653, 490
- Wang, X., et al. 2009a, *ApJ*, 697, 380
- Wang, X., et al. 2009b, *ApJ*, 699, L139
- Wood-Vasey, W. M., et al. 2008, *ApJ*, 689, 377
- Yamanaka, M., et al. 2009, *ApJ*, 707, L118

Yuan, F., et al. 2010, ApJ, 715, 1338

Table 1. Properties of SN 2001ay and its Host Galaxy

Parameter	Value
Host galaxy	IC 4423
Host-galaxy type ^a	Sbc
Heliocentric radial velocity ^b	9067 km s ⁻¹
CMB-frame radial velocity ^c	9266 km s ⁻¹
Distance modulus ^d	35.55 ± 0.1 mag
$E(B - V)_{\text{Gal}}$	0.026 ± 0.006 mag
$E(B - V)_{\text{host}}$	0.072 ± 0.008 mag
SN α (J2000)	14 ^h 26 ^m 17 ^s .0
SN δ (J2000)	+26°14′55″.8
Offset from nucleus	10′.3 W 9′.3 N
Julian Date of B -band maximum	2,452,022.49 ± 0.8
UT Date of B -band maximum	2001 April 23.0
$\Delta m_{15}(B)$	0.68 ± 0.05 mag
$M_B(\text{max})$	−19.19 ± 0.12
$M_V(\text{max})$	−19.17 ± 0.10
$M_R(\text{max})$	−19.10 ± 0.10
$M_I(\text{max})$	−18.90 ± 0.10
$M_J(\text{max})$	−18.77 ± 0.10
$M_H(\text{max})$	−18.62 ± 0.10

^aFrom HyperLEDA.

^bBeers et al. (1995), via NED.

^cFrom NED.

^dUsing $H_0 = 72 \text{ km s}^{-1} \text{ Mpc}^{-1}$ (Freedman et al. 2001).

Table 2. Optical Field-Star Sequence near SN 2001ay^a

ID ^b	U (mag)	B (mag)	V (mag)	R (mag)	I (mag)
1	17.112 (0.043)	16.399 (0.019)	15.480 (0.008)	14.859 (0.018)	14.386 (0.015)
2	18.224 (0.047)	17.262 (0.020)	16.193 (0.007)	15.467 (0.019)	14.921 (0.016)
3	16.705 (0.022)	16.846 (0.019)	16.367 (0.008)	15.981 (0.022)	15.622 (0.021)
4	17.933 (0.035)	18.271 (0.030)	17.864 (0.005)	17.503 (0.025)	17.131 (0.025)
5	19.246 (0.174)	18.729 (0.027)	17.884 (0.015)	17.302 (0.024)	16.796 (0.033)
6	16.813 (0.031)	16.853 (0.017)	16.320 (0.007)	15.917 (0.017)	15.574 (0.014)
7	20.437 (0.129)	19.585 (0.015)	18.313 (0.010)	17.487 (0.017)	16.730 (0.010)
8	20.137 (0.230)	19.987 (0.196)	18.674 (0.070)	18.110 (0.100)	17.467 (0.111)
9	21.270 (0.289)	19.802 (0.108)	18.790 (0.059)	18.009 (0.101)	17.467 (0.074)
10	20.719 (0.155)	18.930 (0.061)

^aMagnitude uncertainties (1σ) are given in parentheses.

^bThe IDs are the same as in Fig. 1. Star 10, located $18.4''$ SE of Star 7, is not visible in the V -band finder.

Table 3. Infrared Field Star Sequence near SN 2001ay^a

ID ^b	J_s (mag)	H (mag)
1	13.718 (0.014)	13.251 (0.011)
6	15.153 (0.021)	14.881 (0.008)
7	15.869 (0.007)	15.281 (0.007)
8	16.566 (0.030)	15.932 (0.031)
10	17.838 (0.024)	17.359 (0.029)

^aMagnitude uncertainties (1σ) are given in parentheses.

^bThe IDs are the same as in Fig. 1 and Table 2.

Table 4. Fully Corrected Optical Photometry of SN 2001ay^a

JD ^b	<i>U</i> (mag)	<i>B</i> (mag)	<i>V</i> (mag)	<i>R</i> (mag)	<i>I</i> (mag)	Telescope ^c	Subs ^d
2020.78	...	16.773 (0.043)	16.708 (0.010)	16.694 (0.015)	16.771 (0.017)	1	N
2021.71	16.419 (0.034)	16.731 (0.020)	16.700 (0.010)	16.695 (0.006)	16.802 (0.010)	1	N
2022.90	...	16.687 (0.050)	16.643 (0.020)	16.635 (0.040)	16.783 (0.050)	2	Y
2023.88	...	16.724 (0.070)	16.640 (0.020)	16.661 (0.030)	16.781 (0.020)	2	Y
2024.89	...	16.709 (0.040)	16.647 (0.020)	16.626 (0.020)	16.829 (0.030)	2	Y
2025.89	...	16.737 (0.030)	16.666 (0.020)	16.692 (0.020)	16.868 (0.050)	2	Y
2026.86	...	16.766 (0.020)	16.664 (0.020)	16.659 (0.030)	16.855 (0.040)	2	Y
2028.89	...	16.841 (0.100)	16.699 (0.080)	2	Y
2030.88	...	16.913 (0.040)	16.734 (0.020)	16.775 (0.030)	16.937 (0.040)	2	Y
2032.88	...	17.065 (0.050)	16.799 (0.030)	16.860 (0.030)	16.952 (0.050)	2	Y
2037.88	...	17.290 (0.050)	16.939 (0.030)	16.948 (0.020)	17.102 (0.040)	2	Y
2039.86	...	17.535 (0.080)	16.945 (0.050)	16.963 (0.040)	17.057 (0.070)	2	Y
2041.80	...	17.647 (0.040)	17.089 (0.050)	2	Y
2043.85	17.143 (0.020)	16.968 (0.020)	17.093 (0.050)	2	Y
2045.86	...	17.952 (0.050)	17.266 (0.030)	17.006 (0.020)	17.024 (0.040)	2	Y
2047.84	...	18.134 (0.040)	17.298 (0.040)	17.015 (0.030)	16.969 (0.040)	2	Y
2051.81	...	18.250 (0.050)	17.424 (0.030)	17.123 (0.020)	16.902 (0.040)	2	Y
2059.81	...	18.554 (0.080)	17.794 (0.040)	17.385 (0.020)	17.138 (0.040)	2	Y
2064.83	...	18.773 (0.080)	18.064 (0.070)	17.629 (0.040)	17.251 (0.060)	2	Y
2069.79	...	19.025 (0.070)	18.117 (0.060)	17.813 (0.030)	17.506 (0.060)	2	Y
2074.74	...	19.071 (0.070)	18.219 (0.070)	18.008 (0.030)	17.805 (0.060)	2	Y
2075.81	...	18.993 (0.060)	18.153 (0.060)	18.099 (0.050)	17.604 (0.050)	2	Y
2079.75	18.250 (0.070)	18.180 (0.050)	17.804 (0.060)	2	Y
2022.99	...	16.709 (0.033)	16.655 (0.013)	16.693 (0.011)	16.758 (0.016)	3	Y
2024.91	...	16.795 (0.044)	16.629 (0.025)	16.686 (0.011)	16.781 (0.027)	3	Y
2029.81	...	16.958 (0.060)	16.716 (0.010)	16.781 (0.010)	16.910 (0.015)	3	Y
2036.86	...	17.322 (0.020)	16.932 (0.010)	16.901 (0.023)	17.007 (0.024)	3	N
2037.83	17.503 (0.040)	17.348 (0.019)	16.990 (0.010)	16.967 (0.018)	17.099 (0.020)	3	N
2038.77	...	17.488 (0.009)	...	17.043 (0.010)	17.079 (0.010)	3	N
2040.79	17.655 (0.031)	17.578 (0.014)	17.054 (0.010)	16.964 (0.016)	16.939 (0.016)	3	N
2041.84	...	17.668 (0.034)	17.003 (0.020)	16.949 (0.033)	16.910 (0.034)	3	N
2043.78	...	17.784 (0.010)	...	16.990 (0.010)	16.845 (0.017)	3	N
2046.82	17.107 (0.010)	16.871 (0.010)	3	N
2050.82	...	18.269 (0.013)	...	16.992 (0.085)	16.816 (0.010)	3	N
2063.76	18.083 (0.017)	...	17.225 (0.029)	3	N
2140.70	...	20.110 (0.130)	19.520 (0.100)	19.390 (0.080)	19.030 (0.090)	3	N
2026.74	...	16.841 (0.062)	16.673 (0.040)	4	N
2030.67	...	16.953 (0.017)	16.725 (0.010)	5	N
2046.62	...	18.063 (0.024)	17.194 (0.013)	5	N
2047.65	...	18.209 (0.047)	17.247 (0.027)	5	N
2055.63	17.687 (0.028)	5	N
2052.65	18.633 (0.041)	18.356 (0.023)	17.468 (0.012)	17.152 (0.027)	16.850 (0.029)	6	Y

^aThe *BVRI* data in this table include the K-corrections, S-corrections, and corrections applied to photometry derived using aperture magnitudes without subtraction templates. Magnitude uncertainties (1σ) are given in parentheses.

^bJulian Date *minus* 2,450,000.

^c1 = CTIO 0.9-m, 2 = KAIT, 3 = Nickel 1-m, 4 = Yale-AURA-Lisbon-Ohio (YALO) 1-m, 5 = LCO 2.5-m, and 6 = CTIO 1.5-m telescopes.

^dImage-subtraction templates used? Y = yes; N = No.

Table 5. K-Corrections for SN 2001ay in Optical Bands^a

UT Date (2001)	Phase (d) ^b	Telescope	ΔB (mag)	ΔV (mag)	ΔR (mag)	ΔI (mag)
Apr 21	−2	FLWO 1.5-m	−0.010	−0.031	−0.120	−0.045
Apr 24	+1	FLWO 1.5-m	0.000	−0.028	−0.118	−0.068
Apr 26	+3	MMT 6.5-m	−0.001	−0.020	−0.090	−0.029
Apr 27	+4	FLWO 1.5-m	0.018	−0.014	−0.097	−0.015
Apr 30	+7	FLWO 1.5-m	0.010	−0.017	−0.094	−0.050
May 02	+9	FLWO 1.5-m	0.023	−0.005	−0.093	−0.065
May 10	+17	BAO 2.16-m	...	−0.024:	−0.064	...
May 16	+23	FLWO 1.5-m	0.080	0.047	−0.055	0.042
May 23	+30	FLWO 1.5-m	0.090	0.066	−0.057	0.030
May 24	+31	MMT 6.5-m	0.097	0.077	−0.039	−0.008
May 25	+32	FLWO 1.5-m	0.085	0.068	−0.061	0.025
May 25	+32	MMT 6.5-m	0.100	0.081	−0.040	0.022
May 30	+37	FLWO 1.5-m	0.082	0.070	−0.049	0.019
Jun 18	+56	FLWO 1.5-m	0.089	0.073	−0.067	0.043
Jun 18	+56	MMT 6.5-m	0.093	0.070	−0.056	0.059

^aThese corrections (measured in magnitudes) are *subtracted* from the photometric data to correct the photometry to the rest frame. These were calculated using the Bessell (1990) filter profiles.

^bThe number of observer-frame days since the time of B maximum, 2001 April 23.

Table 6. Interpolated Corrections to Optical Photometry^a

JD ^b	K _{CB}	K _{CV}	K _{CR}	K _{CI}	S _{CB}	S _{CV}	S _{CR}	S _{CI}	Telescope ^c
2020.78	−0.010	−0.031	−0.120	−0.053	−0.008	−0.003	−0.006	−0.002	1
2021.71	−0.006	−0.030	−0.116	−0.052	−0.007	−0.004	−0.005	−0.006	1
2022.90	−0.005	−0.028	−0.113	−0.050	−0.008	−0.005	0.022	−0.017	2
2023.88	−0.002	−0.025	−0.110	−0.048	−0.008	−0.005	0.021	−0.017	2
2024.89	0.004	−0.022	−0.106	−0.046	−0.007	−0.005	0.020	−0.017	2
2025.89	0.006	−0.021	−0.103	−0.044	−0.007	−0.005	0.019	−0.016	2
2026.86	0.007	−0.019	−0.100	−0.041	−0.007	−0.005	0.019	−0.016	2
2028.89	0.013	−0.013	−0.006	−0.004	2
2030.88	0.022	−0.006	−0.088	−0.033	−0.005	−0.002	0.017	−0.016	2
2032.88	0.030	0.000	−0.083	−0.028	−0.005	−0.001	0.017	−0.016	2
2037.88	0.045	0.016	−0.071	−0.017	−0.005	0.005	0.017	−0.015	2
2039.86	0.050	0.022	−0.066	−0.012	−0.005	0.007	0.017	−0.015	2
2041.80	0.057	0.029	−0.006	0.008	2
2043.85	...	0.037	−0.059	−0.007	...	0.010	0.019	−0.014	2
2045.86	0.071	0.045	−0.056	0.002	−0.007	0.011	0.020	−0.014	2
2047.84	0.078	0.053	−0.054	0.007	−0.008	0.011	0.021	−0.014	2
2051.81	0.089	0.068	−0.050	0.015	−0.011	0.012	0.023	−0.013	2
2059.81	0.089	0.075	−0.048	0.031	−0.017	0.009	0.027	−0.011	2
2064.83	0.089	0.073	−0.050	0.039	−0.018	0.007	0.029	−0.010	2
2069.79	0.087	0.067	−0.053	0.045	−0.018	0.004	0.030	−0.009	2
2074.74	0.088	0.066	−0.058	0.048	−0.011	0.005	0.030	−0.007	2
2075.81	0.088	0.067	−0.059	0.049	−0.009	0.005	0.030	−0.007	2
2079.75	...	0.072	−0.062	0.050	...	0.010	0.028	−0.006	2
2022.99	−0.005	−0.028	−0.113	−0.050	0.003	−0.009	0.024	0.027	3
2024.91	0.004	−0.022	−0.106	−0.046	0.004	−0.008	0.023	0.036	3
2029.81	0.017	−0.010	−0.091	−0.035	0.000	−0.002	0.022	0.060	3
2036.86	0.042	0.013	−0.073	−0.019	−0.014	0.007	0.024	0.073	3
2037.83	0.045	0.016	−0.071	−0.017	−0.016	0.008	0.024	0.076	3
2038.77	0.047	...	−0.068	−0.014	−0.018	...	0.024	0.079	3
2040.79	0.053	0.026	−0.064	−0.010	−0.022	0.011	0.024	0.082	3
2041.84	0.057	0.029	−0.063	−0.007	−0.024	0.011	0.024	0.082	3
2043.78	0.064	...	−0.059	−0.003	−0.028	...	0.024	0.082	3
2046.82	−0.056	0.004	0.025	0.075	3
2050.82	0.087	...	−0.051	0.013	−0.037	...	0.027	0.053	3
2063.76	...	0.074	...	0.037	...	−0.005	...	0.000	3
2026.74	0.007	−0.019	4
2030.67	0.008	−0.006	5
2046.62	0.075	0.049	5
2047.65	0.078	0.053	5
2055.63	...	0.075	5
2052.66	0.089	0.068	−0.050	0.017	0.018	0.006	0.000	−0.028	6

^aValues in Columns 2 through 9 are in magnitudes. The K-corrections are subtracted from the data in Table 4. The S-corrections are added to the data in Table 4.

^bJulian Date *minus* 2,450,000.

^c1 = CTIO 0.9-m, 2 = KAIT, 3 = Nickel 1-m, 4 = Yale-AURA-Lisbon-Ohio (YALO) 1-m, 5 = LCO 2.5-m, and 6 = CTIO 1.5-m telescopes.

Table 7. Near-Infrared Photometry of SN 2001ay^a

JD ^b	J_s (mag)	H (mag)	Telescope ^c
2024.73	...	17.045 (0.042)	1
2025.67	16.977 (0.032)	16.893 (0.044)	1
2026.70	17.050 (0.028)	...	1
2029.70	17.132 (0.022)	17.000 (0.035)	1
2031.68	17.136 (0.022)	16.965 (0.036)	1
2032.70	17.190 (0.028)	17.110 (0.027)	1
2045.66	17.291 (0.024)	16.873 (0.020)	2
2047.65	17.509 (0.049)	...	1
2049.66	17.396 (0.035)	16.853 (0.039)	1
2051.65	17.430 (0.034)	16.894 (0.038)	1
2053.67	17.337 (0.031)	...	1
2055.67	17.387 (0.031)	17.078 (0.056)	1
2056.67	17.420 (0.031)	16.998 (0.022)	1
2061.65	...	16.905 (0.022)	2
2068.57	17.592 (0.033)	17.157 (0.028)	2

^aMagnitude uncertainties (1σ) are given in parentheses.

^bJulian Date *minus* 2,450,000.

^c1 = LCO 1-m, 2 = LCO 2.5-m telescopes.

Table 8. Spectroscopic Observations in the “CfA Set”

UT Date (2001)	Julian Day	Tel.	Range (Å)	Res. (Å)	Pos.A. (°)	Par.A. (°)	Airmass	Flux Std.	Sky	Seeing ($''$)	Slit ($''$)	Exp. (s)	Observer(s)
Apr 21.48	2452020.98	FLWO	3720–7540	7.0	71.00	70.02	1.48	Feige34		1–2	3	1200	Calkins
Apr 24.31	2452023.81	FLWO	3720–7540	7.0	0.00	−16.25	1.01	Feige34	clear	2	3	1200	Berlind
Apr 26.33	2452025.83	FLWO	3720–7540	7.0	45.00	43.51	1.01	Feige34	some clouds	1–2	3	1200	Berlind
Apr 26.40	2452025.90	MMTO	3250–8900	8.0	Par.A.	71.15	1.12	Feige34/BD26				900	Matheson
Apr 26.41	2452025.91	MMTO	3250–8900	8.0	Par.A.	71.52	1.15	Feige34/BD26				900	Matheson
Apr 27.36	2452026.86	FLWO	3720–7540	7.0	64.00	65.79	1.04	HZ44		1–2	3	1200	Calkins
Apr 30.36	2452029.86	FLWO	3720–7540	7.0	70.00	67.86	1.05	Feige34	clear	1–2	3	1200	Berlind
May 02.29	2452031.79	FLWO	3720–7540	7.0	−9.00	−19.75	1.01	HZ44	clear	1–2	3	1200	Berlind
May 16.26	2452045.76	FLWO	3720–7540	7.0	−33.00	−13.29	1.01	HZ44	clear	1–2	3	1200	Calkins
May 23.33	2452052.83	FLWO	3720–7540	7.0	69.00	71.42	1.14	Feige34	cirrus	2	3	1200	Rines
May 24.32	2452053.82	MMTO	3220–8900	8.0	at Par.A.	70.92	1.11	BD28/BD26	clear			1200	Challis, Phelps
May 24.33	2452053.83	MMTO	4950–10000	8.0	Par.A.	71.51	1.16	BD26	clear			1200	Challis, Phelps
May 25.32	2452054.82	MMTO	3220–8900	8.0	Par.A.	71.36	1.14	Feige34/BD26	clear			1800	Challis
May 25.35	2452054.85	MMTO	4950–10000	8.0	Par.A.	71.52	1.23	BD26	clear			1800	Challis
May 25.37	2452054.87	FLWO	3720–7500	7.0	69.00	70.63	1.39	Feige34	cirrus	2	3	1200	Rines
May 30.36	2452059.86	FLWO	3720–7540	7.0	71.00	70.51	1.40	HZ44	clear	1–2	3	1200	Calkins
May 30.38	2452059.88	FLWO	3720–7540	7.0	71.00	69.68	1.53	HZ44	cirrus	1–2	3	1200	Calkins
June 18.22	2452078.72	FLWO	3720–7540	7.0	69.00	66.99	1.05	HZ44	clouds	1–2	3	1200	Berlind
June 18.29	2452078.79	MMTO	3200–8900	8.0	Par.A.	71.24	1.29	BD28/BD26	some clouds			900	Matheson
June 18.30	2452078.80	MMTO	3200–8900	8.0	Par.A.	70.84	1.35	BD28/BD26	some clouds			900	Matheson

Table 9. Other Spectroscopic Observations

UT Date (2001)	Phase (d) ^a	Telescope	Wavelength Range (Å)	Resolution (Å)
Apr 22	−1	Keck II 10-m	3922–10000	1.25
Apr 29	+6	KPNO 2.1-m	5350–[9500]	4.8
Apr 30	+7	Lick 3-m	3260–10600	5.5/10.5
May 01	+8	LCO 2.5-m	3500–9199	7.0
May 02	+9	<i>HST</i> 2.4-m	2877–5348	3.55 to 4.10
May 09	+16	<i>HST</i> 2.4-m	2930–5695	3.55 to 4.10
May 10	+17	BAO 2.16-m	4100–9000	9.6
May 16	+23	Lick 3-m	3300–10450	5.5/10.5
May 17	+24	LCO 2.5-m	3500–9350	7.0
May 20	+27	BAO 2.16-m	3450–9000	9.6
May 23	+30	KPNO 4.0-m	3500–5493/5300–11600	7.8/13.8
May 25	+32	BAO 2.16-m	3700–9300	9.6
May 26	+33	LCO 2.5-m	3800–9234	7.0
May 30	+37	BAO 2.16-m	3970–8200	4.8

^aNumber of observer frame days since time of *B*-band maximum, 2001 April 23.

Table 10. Comparison of Three Objects

Parameter	SN 2001ay	SN 2005eq	SN 2009dc
$\Delta m_{15}(B)$	0.68 (0.05)	0.72–0.78	0.72 (0.03)
$M_V(\text{max})$	−19.17 (0.10)	−19.40 (0.08)	−20.16 (0.10)
Si II velocity ^a (km s ^{−1})	−14,340 [−1.5 d]	−10,200 [−5 d]	−8600 [−7 d]
C II line(s)	weak	not detectable	very strong
<i>H</i> -band light curve	flat	peaked early	increasing

^aFor the $\lambda_0 = 6355$ Å line. The values in brackets correspond to the numbers of rest-frame days after the time of *B* maximum when the line was measured at this velocity. For SN 2009dc the velocity is from Silverman et al. (2010).

Fig. 1.— Finder chart for IC 4423, SN 2001ay, and some field stars in our Galaxy.

Fig. 2.— K-corrections for $BVRI$ photometry of SN 2001ay.

Fig. 3.— S-corrections for B - and V -band photometry of SN 2001ay.

Fig. 4.— Effective I -band transmission functions for the Bessell (1990) filter, the KAIT filter, and the Nickel 1-m filter.

Fig. 5.— S-corrections for R - and I -band photometry of SN 2001ay.

Fig. 6.— Comparison of the B - and V -band light curves of SNe 2001ay, 2005eq (Contreras et al. 2010), and 2009dc (Silverman et al. 2010).

Fig. 7.— Unreddened $B - V$ colors of SN 2001ay vs. time since B -band maximum.

Fig. 8.— Similar to Figure 6, except for the R and I bands.

Fig. 9.— Near-IR photometry of SNe 2009dc (Stritzinger et al. 2011), 2001ay, and 2005eq (Contreras et al. 2010).

Fig. 10.— Absolute V -band magnitudes at maximum light of six very slowly declining Type Ia SNe vs. the decline-rate parameter $\Delta m_{15}(B)$. The decline-rate relation of Garnavich et al. (2004) is also shown.

Fig. 11.— Near-IR absolute magnitudes at maximum light of Type Ia SNe.

Fig. 12.— Temporal sequence of spectra of SN 2001ay.

Fig. 13.— Additional spectra of SN 2001ay obtained with the Lick Observatory 3-m Shane telescope, *HST*, and the Las Campanas Observatory 2.5-m du Pont telescope.

Fig. 14.— A portion of our highest signal-to-noise ratio spectrum of SN 2001ay, taken with the Keck ESI on 2001 April 22.

Fig. 15.— Profile of the Na I D lines in our Keck ESI spectrum. The Milky Way and host-galaxy components are clearly present.

Fig. 16.— Blueshifted velocity of two Si II lines in the spectra of SN 2001ay around maximum light.

Fig. 17.— Bolometric luminosities (L) of SNe 2001ay, 2007if (Scalzo et al. 2010), and 2009dc (Taubenberger et al. 2011), measured in erg s^{-1} .

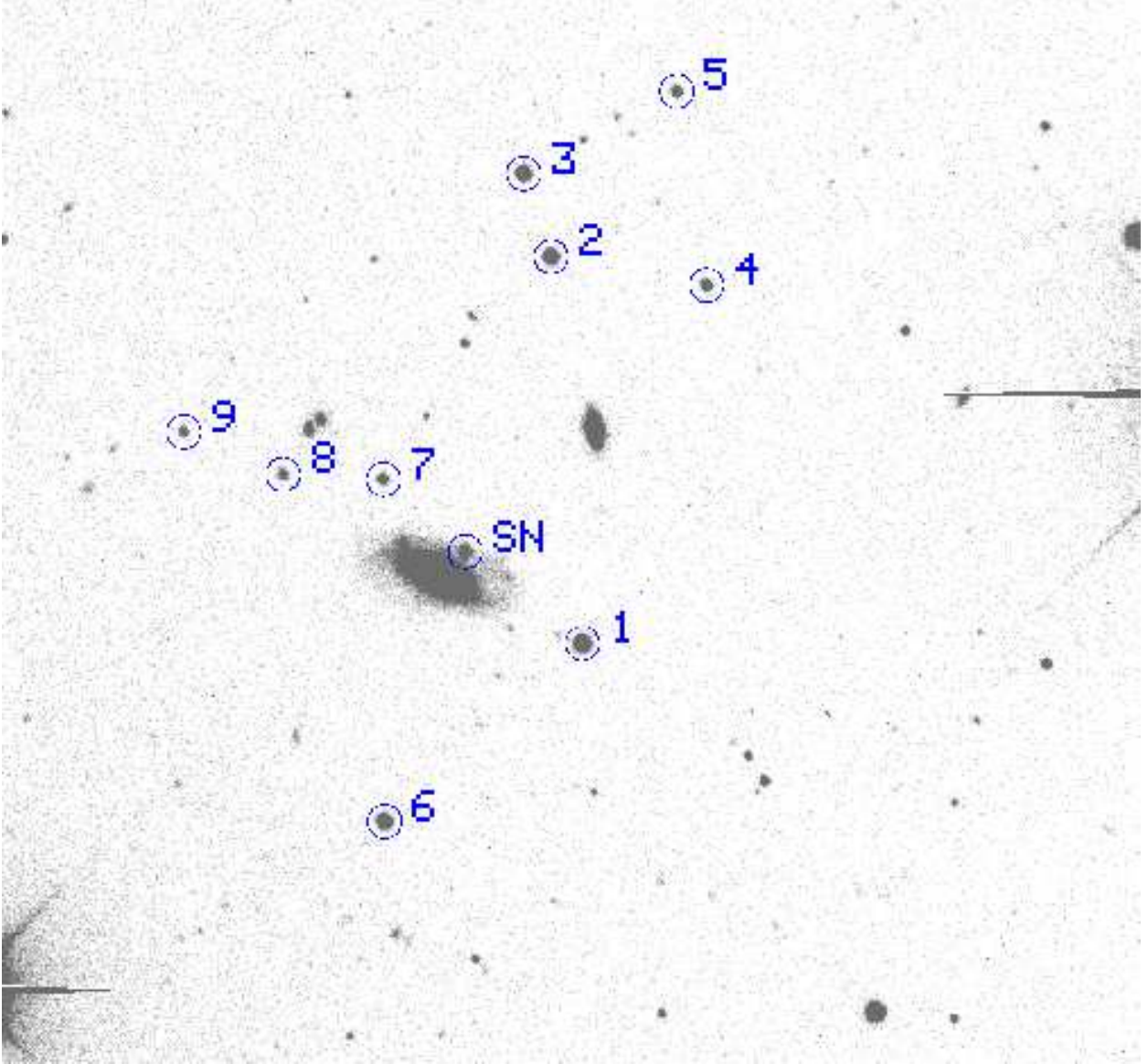
Fig. 18.— The best-fit radioactive decay energy deposition function (middle solid line) to the UVOIR light curve (blue squares) of SN 2001ay.

Fig. 19.— Comparison of the optical spectra of SNe 2001ay, 2005eq, and 2009dc.

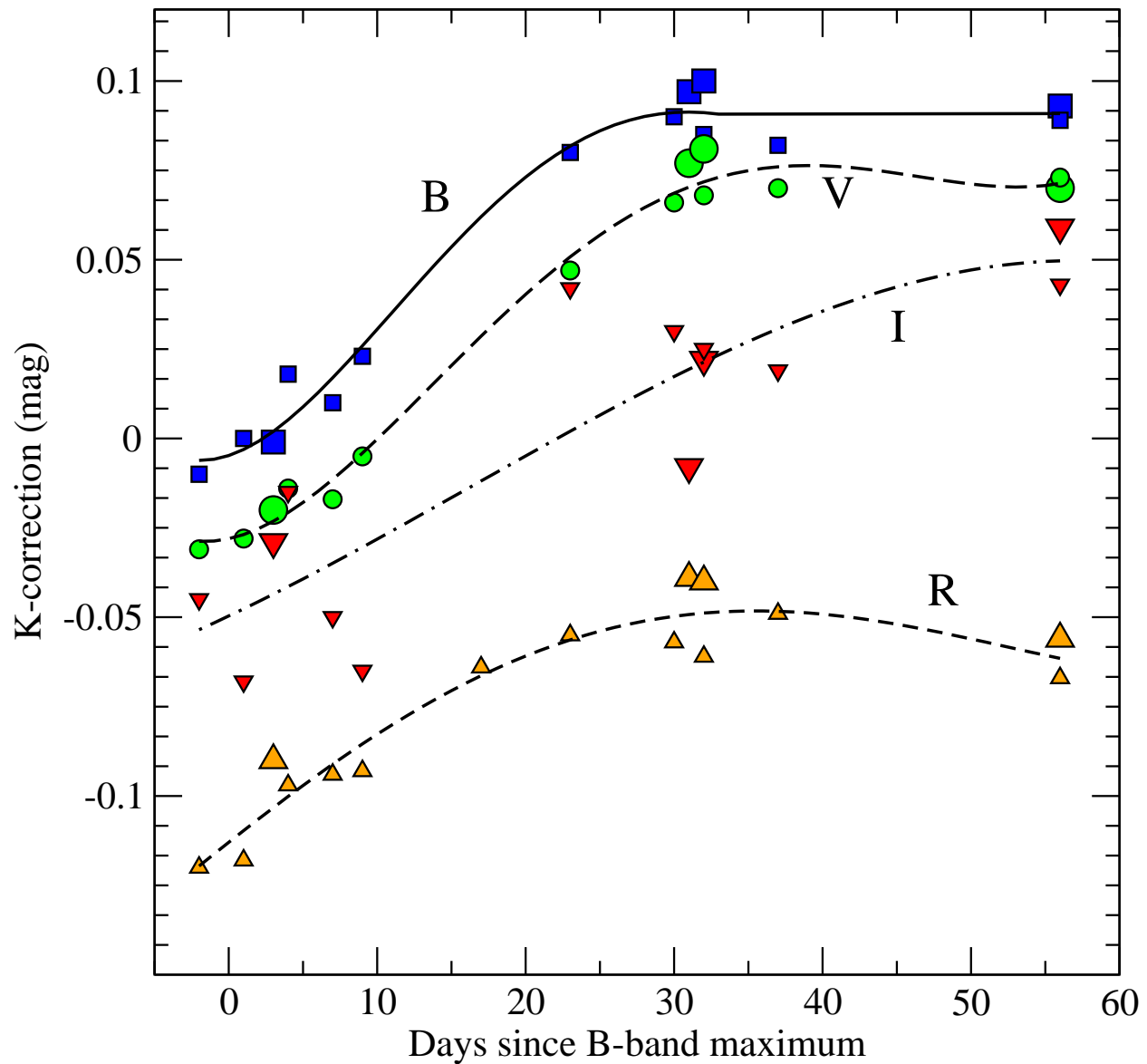
Fig. 20.— SYNOW modeling of the optical spectrum of SN 2001ay at 1 d before B maximum. Upper curve = data; lower curve = SYNOW model. The dashed lines indicate the addition of C II to the model.

Fig. 21.— SYNOW modeling of the optical spectrum of SN 2001ay 6 d after B maximum. Upper curve = data; lower curve = SYNOW model.

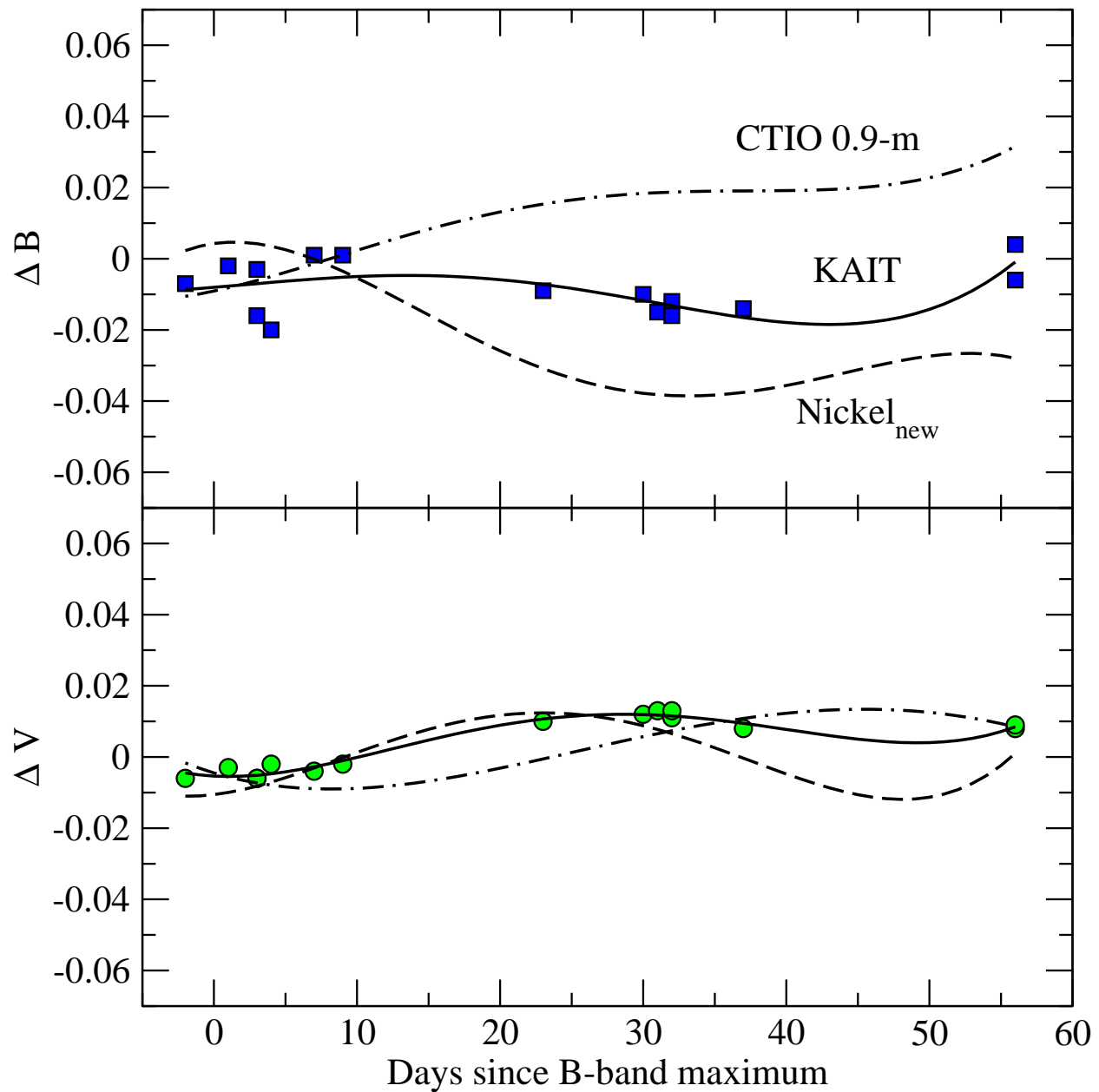
Fig. 22.— SYNAPPS modeling of the optical spectrum of SN 2001ay 1 d before B maximum. The blue dashed line (model spectrum) can be shifted arbitrarily along the vertical axis to match the actual spectrum (shown in black).



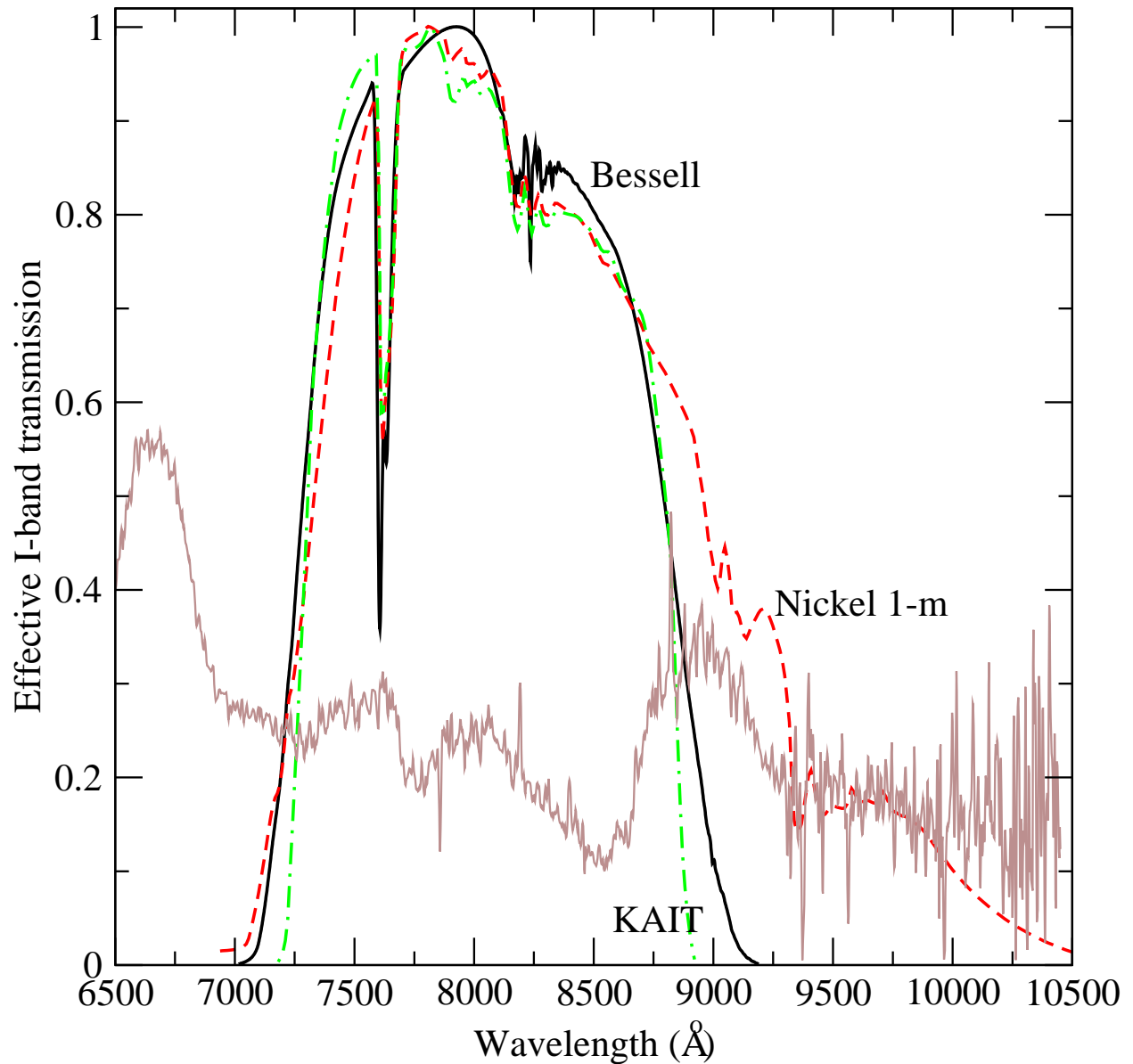
Krisciunas *et al.* Figure 1. Finder chart for IC 4423, SN 2001ay, and some field stars in our Galaxy. This $7.4' \times 7.4'$ image is a 200 s *V*-band exposure obtained on 2001 May 23 with the CTIO 1.5-m telescope. North is up and east is to the left. The SN is located $10.3''$ W and $9.3''$ N of the galaxy core.



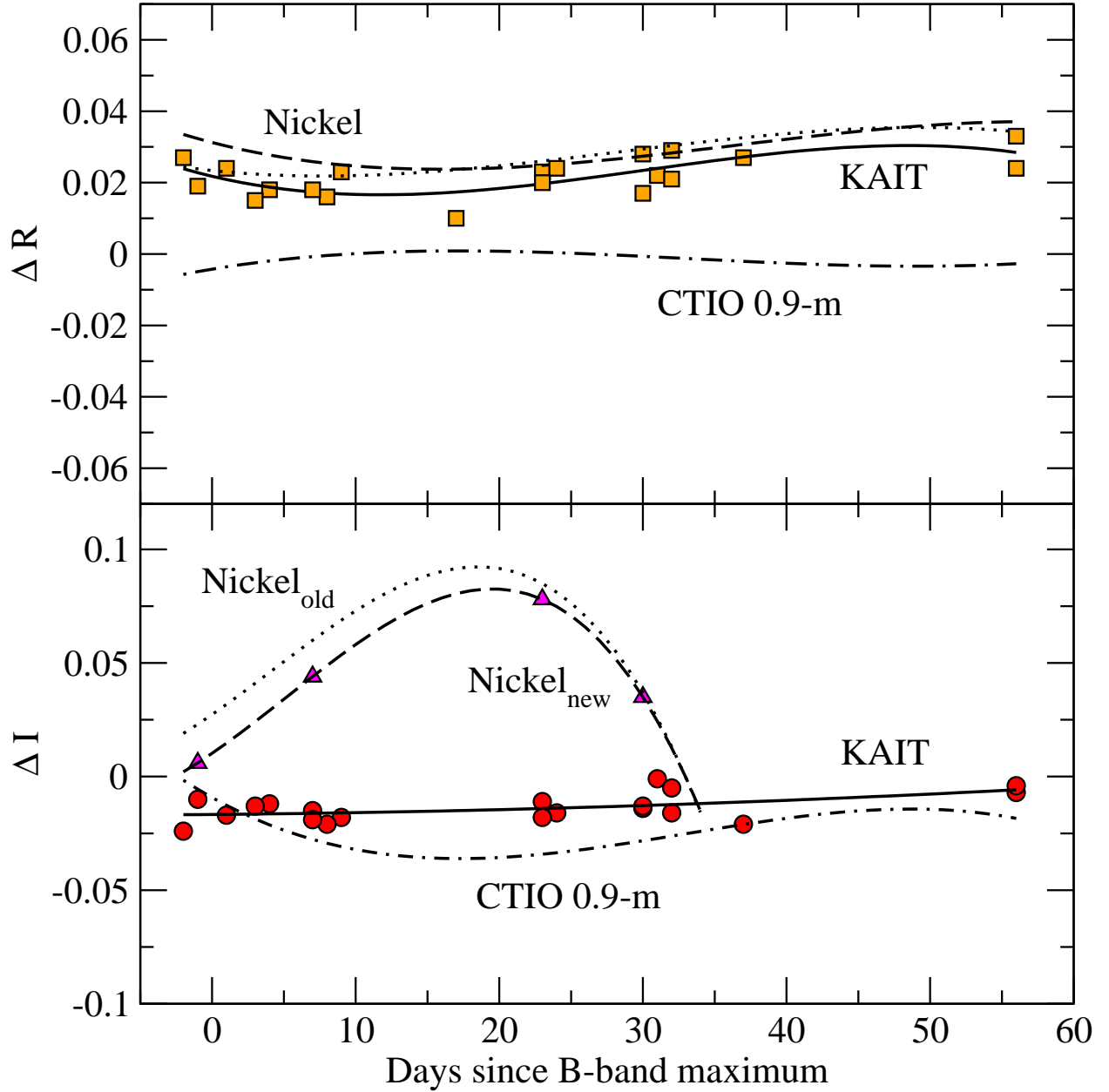
Krisciunas *et al.* Figure 2. K-corrections for *BVRI* photometry of SN 2001ay. These account for the shifting of the SN spectrum to longer wavelengths owing to the redshift of the host galaxy. These values are to be *subtracted* from the photometry. Values derived from the high signal-to-noise ratio MMT spectra are plotted as larger symbols.



Krisciunas *et al.* Figure 3. S-corrections for B - and V -band photometry of SN 2001ay, based on spectra from the FLWO 1.5-m and the MMT. The individual points are shown only for the KAIT corrections. The corrections for the older Nickel 1-m chip are essentially the same as those shown for the newer Nickel 1-m chip. S-corrections are *added* to the photometry to correct it to the filter system of Bessell (1990).



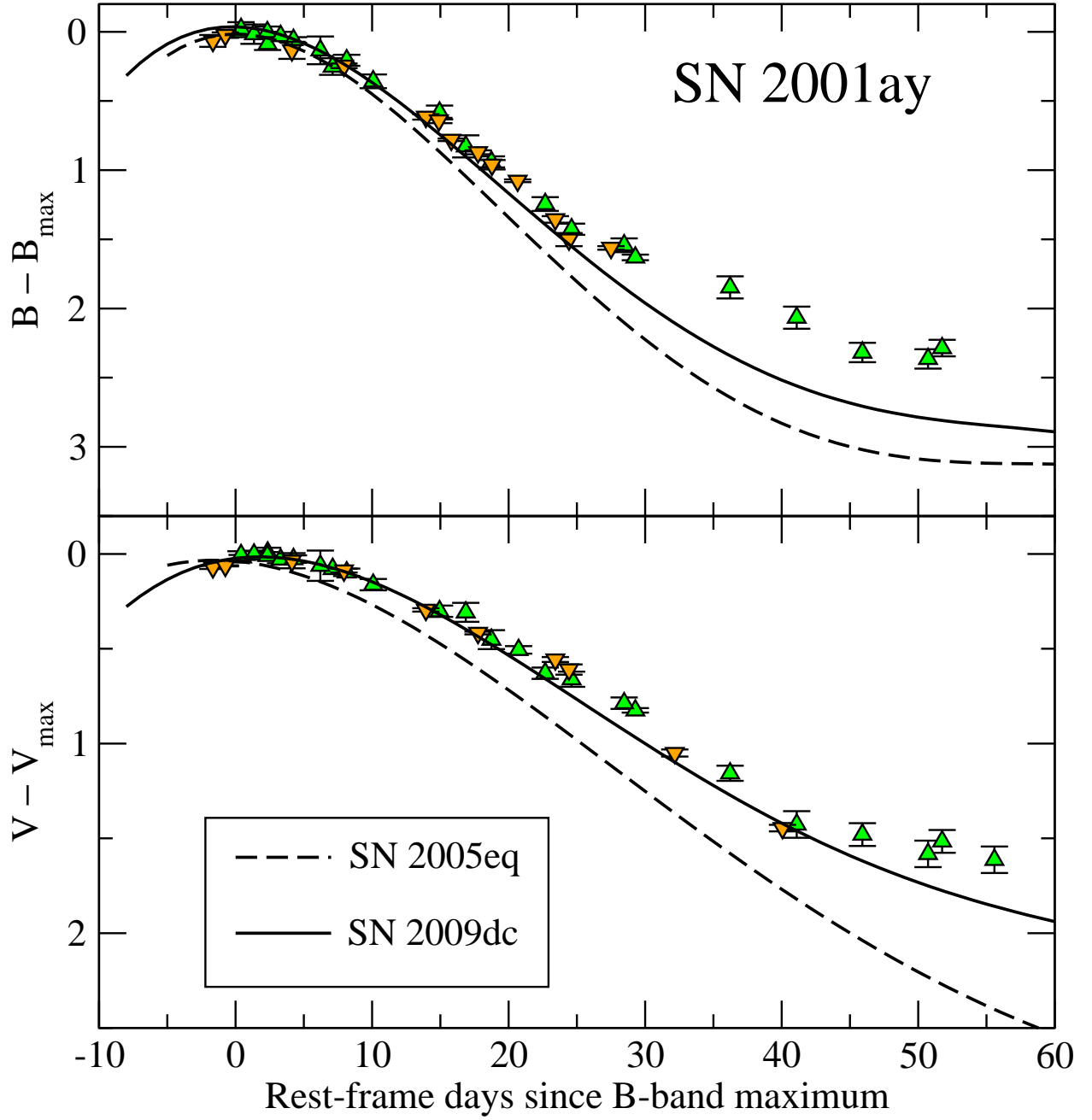
Krisciunas *et al.* Figure 4. Effective *I*-band transmission functions for the Bessell (1990) filter, the KAIT filter, and the Nickel 1-m filter used with the newer, higher quantum efficiency chip. Each filter profile has been normalized to 1.00 at maximum throughput. We also include the $t = +23$ d spectrum from Figure 13 (multiplied by 10^{15}); it shows significant flux past 9000 Å, which is measured by the Lick 1-m system but excluded in the KAIT measurements.



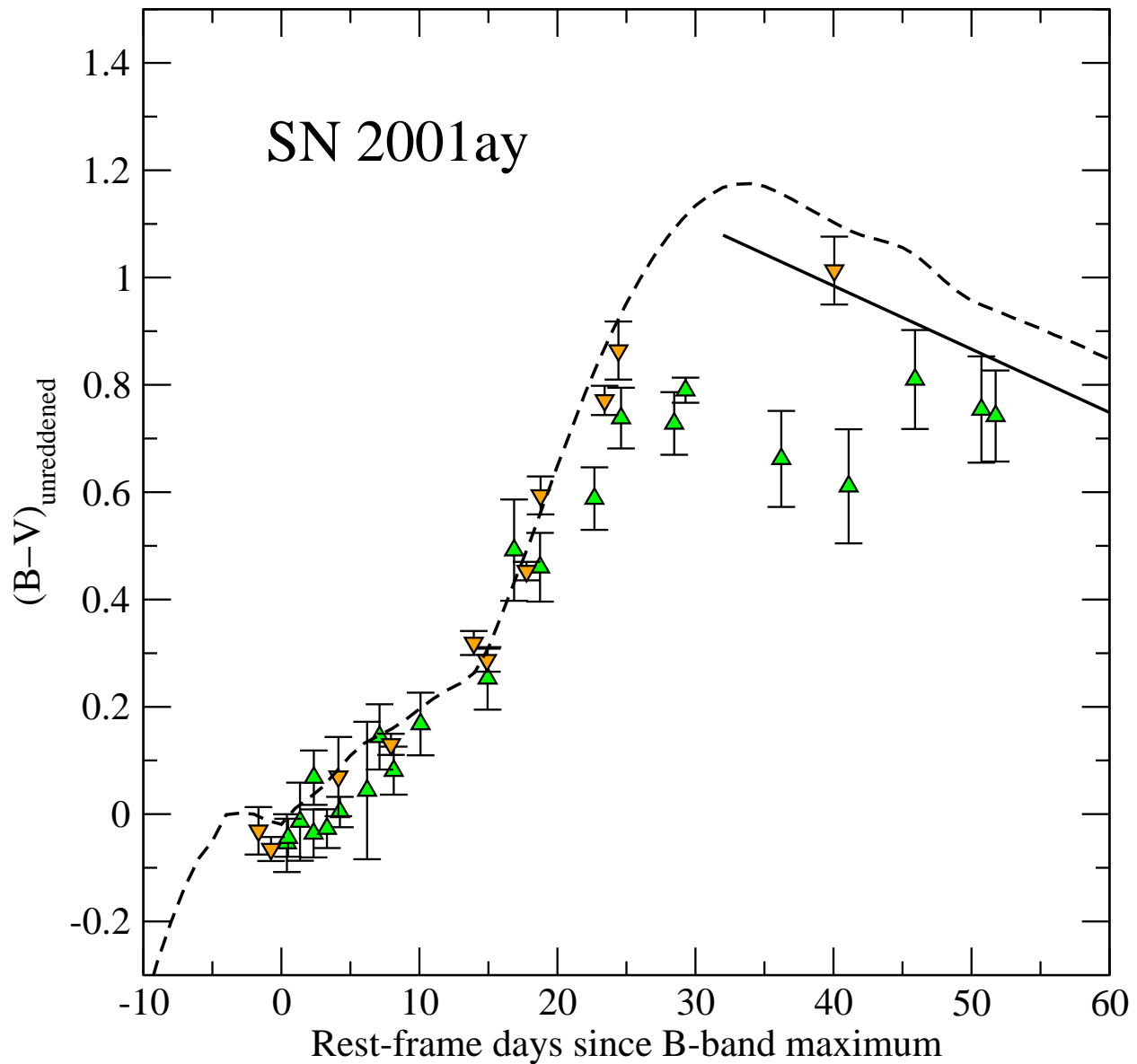
Krisciunas *et al.* Figure 5. S-corrections for R - and I -band photometry of SN 2001ay.

Corrections for the older Nickel 1-m chip are shown as a dotted line; corrections for the new Nickel 1-m chip are shown as a dashed line. For the I -band corrections with the Nickel 1-m filter and both CCD chips used in the camera, we can only use spectra that extend to sufficiently long wavelengths (our Keck spectrum, two spectra taken with the Lick 3-m, and one with the KPNO 4-m). For the Nickel 1-m photometry to match the KAIT photometry, we would need the S-corrections to be a factor of 3 larger than the derived values.

S-corrections are *added* to the photometry to correct it to the filter system of Bessell (1990).

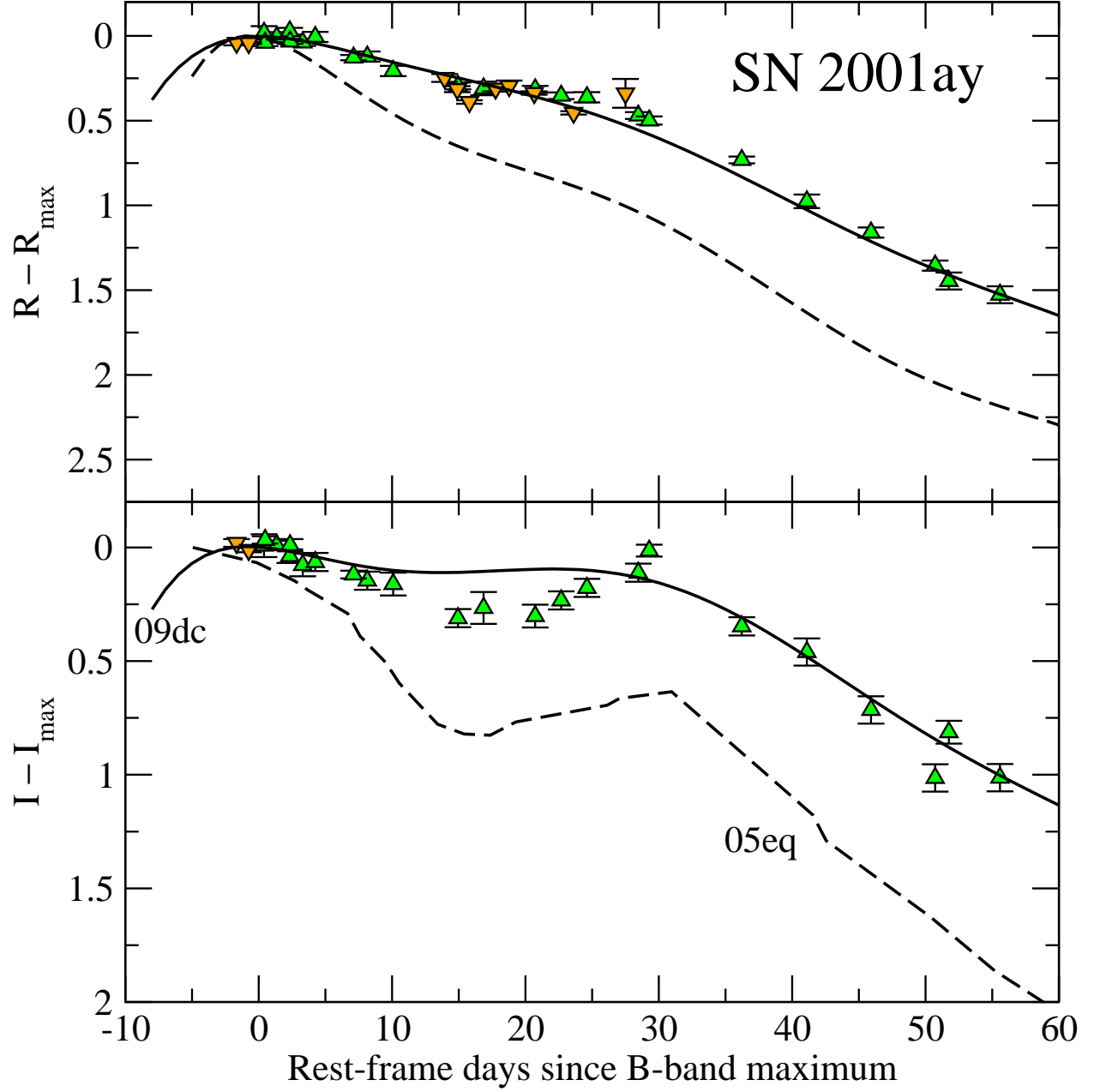


Krisciunas *et al.* Figure 6. Comparison of the B - and V -band light curves of SNe 2001ay, 2005eq (Contreras et al. 2010), and 2009dc (Silverman et al. 2010). The SN 2001ay data are K-corrected and S-corrected, and the CTIO 0.9-m and Nickel 1-m aperture photometry includes additional corrections discussed in the text. For SN 2001ay the upward pointing triangles represent data which result from PSF photometry using image-subtraction templates. The downward pointing triangles are SN 2001ay data based on aperture photometry.

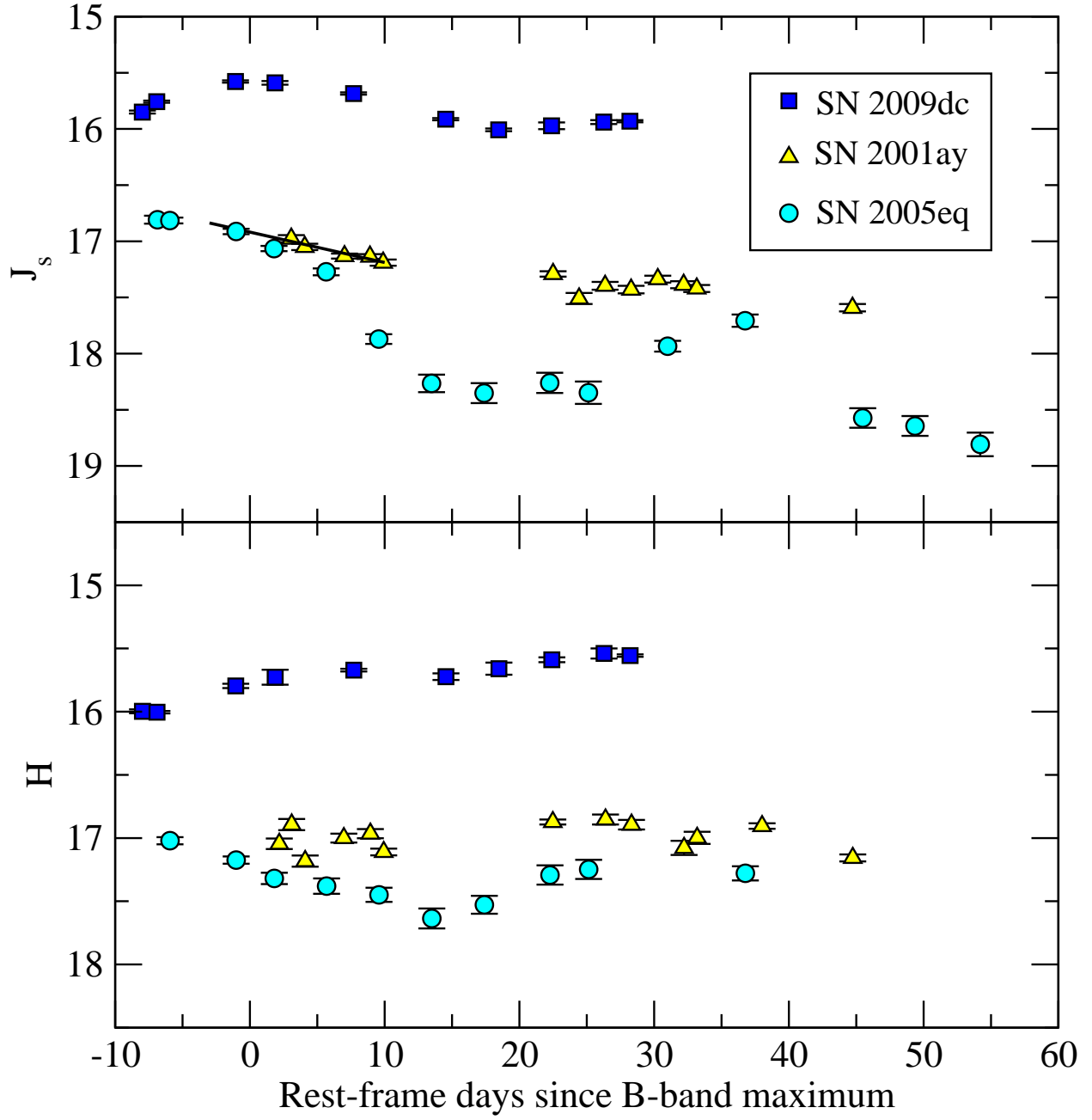


Krisciunas *et al.* Figure 7. Unreddened $B - V$ colors of SN 2001ay vs. time since B -band maximum. Upward pointing triangles are data derived using image-subtraction templates.

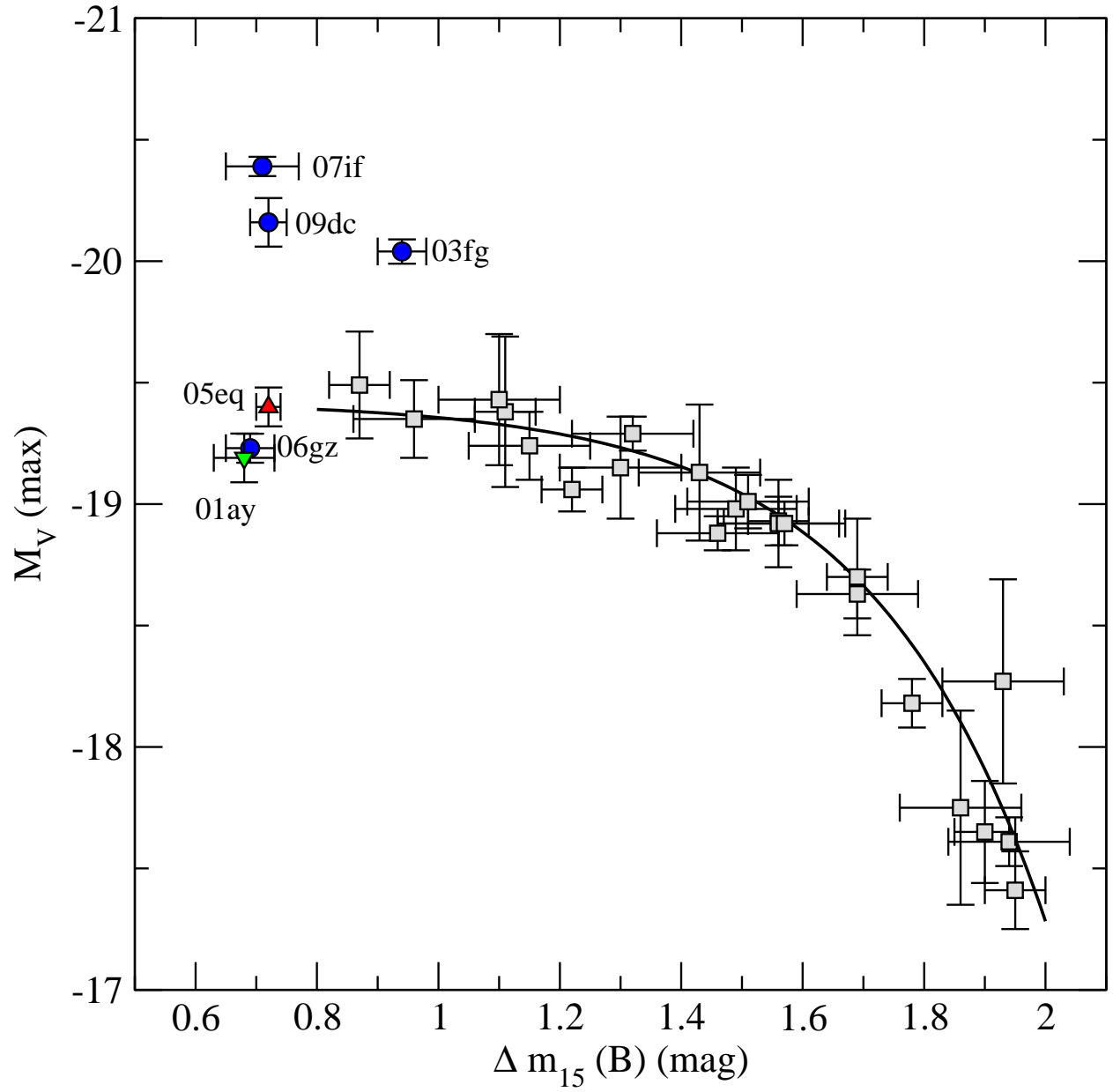
Downward pointing triangles represent data derived from aperture magnitudes without template subtractions. The dashed line is the locus from Prieto, Rest, & Suntzeff (2006b) for their most slowly declining object (with $\Delta m_{15}(B) = 0.83$ mag). The solid line is the commonly used Lira-Phillips locus (Lira 1995; Phillips et al. 1999).



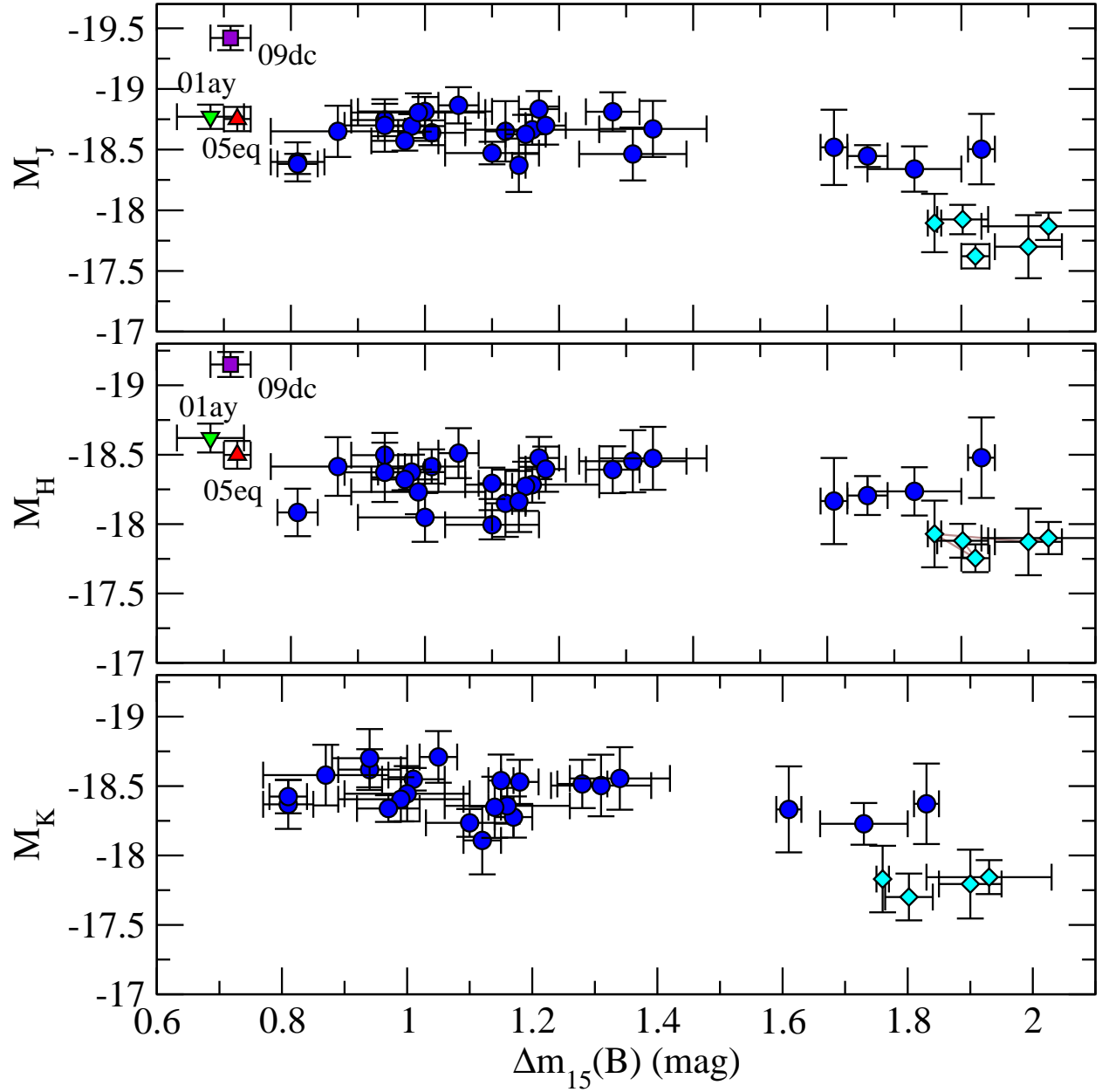
Krisciunas *et al.* Figure 8. Similar to Figure 6, except for the R and I bands. In the case of SN 2005eq the data are taken in Sloan r and i filters, not in Kron-Cousins R and I . The Nickel 1-m I -band data are not shown.



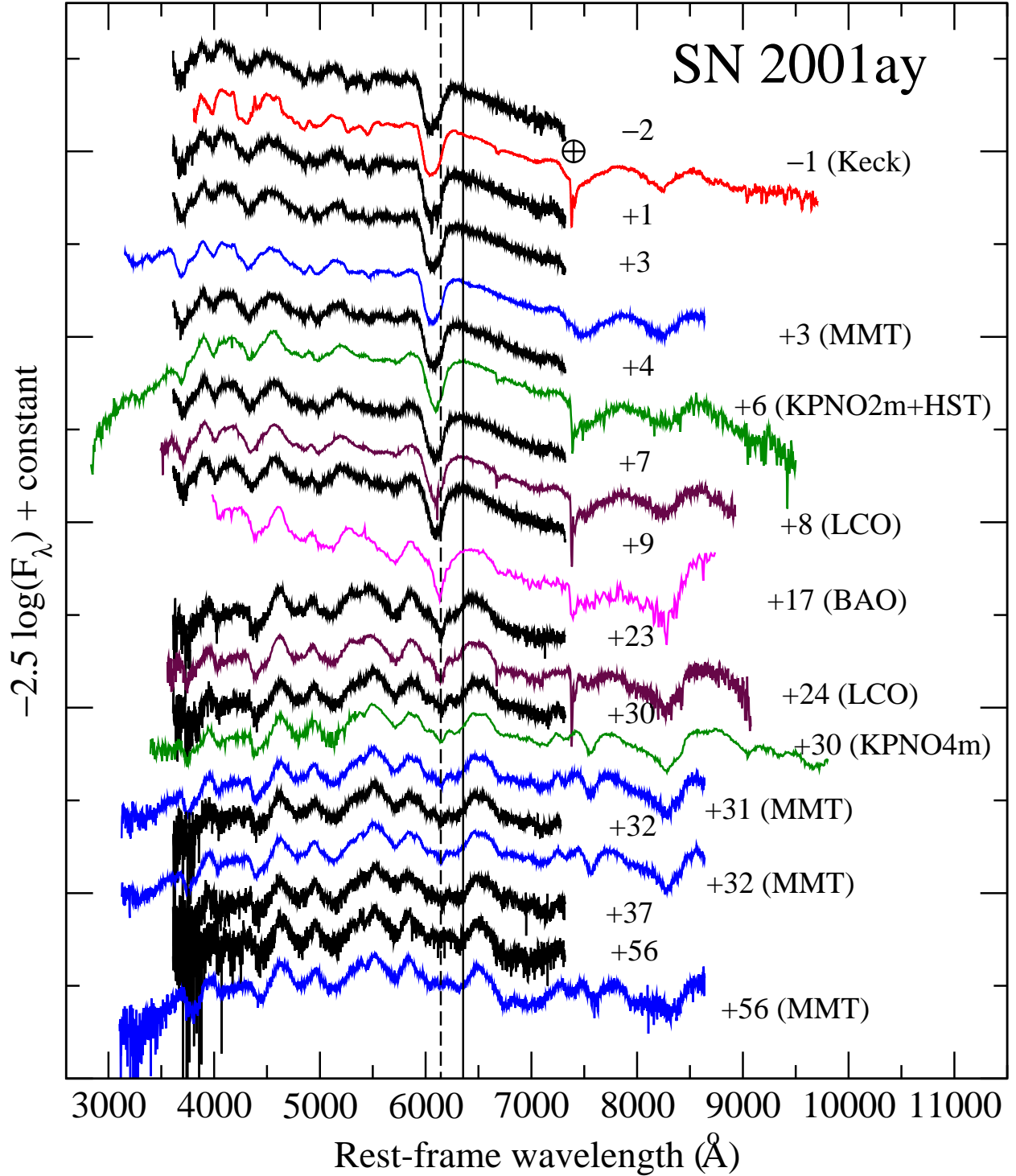
Krisciunas *et al.* Figure 9. Near-IR photometry of SNe 2009dc (Stritzinger et al. 2011), 2001ay, and 2005eq (Contreras et al. 2010). The solid line is an educated guess that SN 2001ay may have been ~ 0.12 mag brighter in J_s at maximum light than our earliest J_s datum.



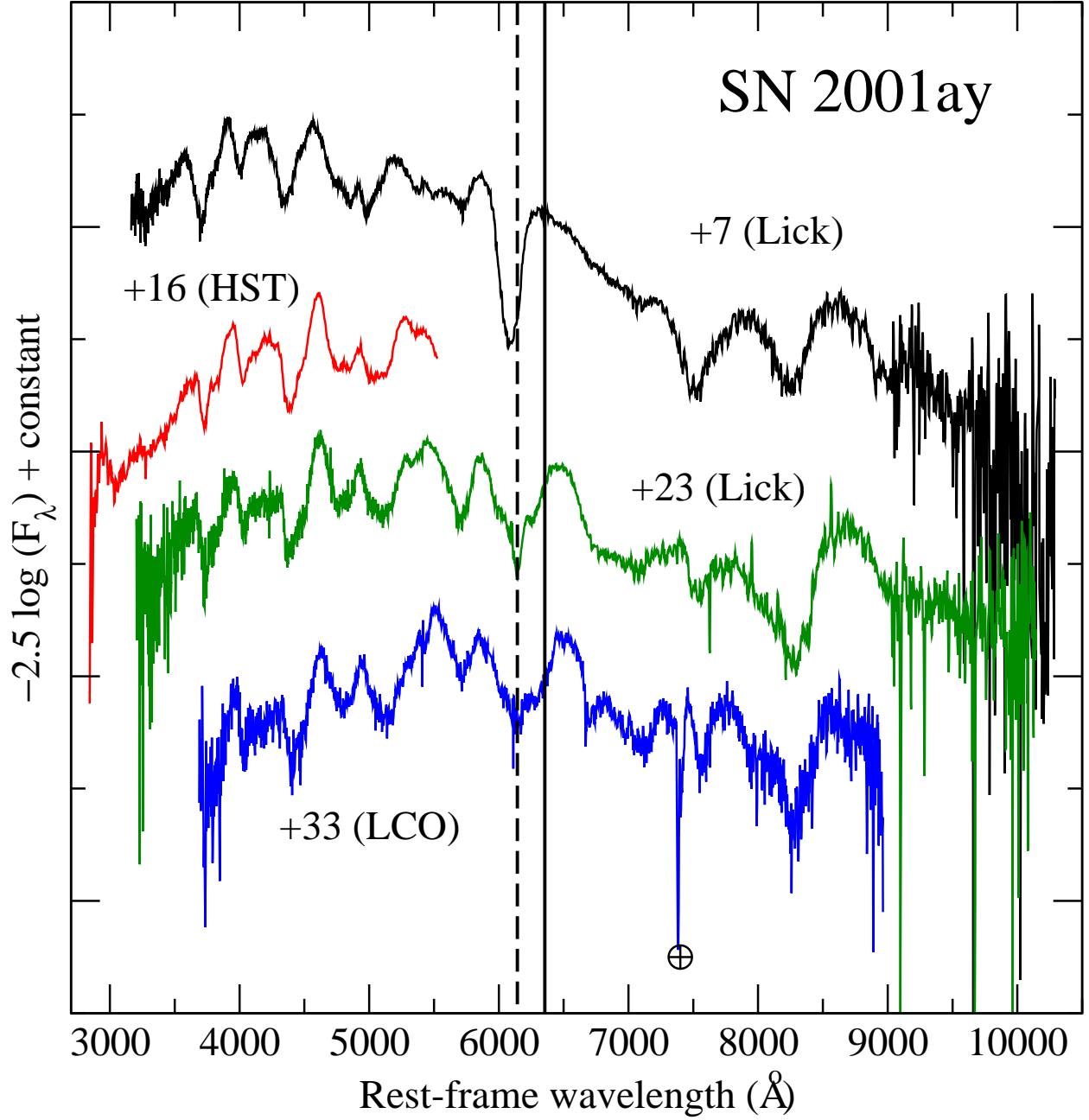
Krisciunas *et al.* Figure 10. Absolute V -band magnitudes at maximum light of six very slowly declining Type Ia SNe vs. the decline-rate parameter $\Delta m_{15}(B)$. The decline-rate relation of Garnavich et al. (2004) is also shown.



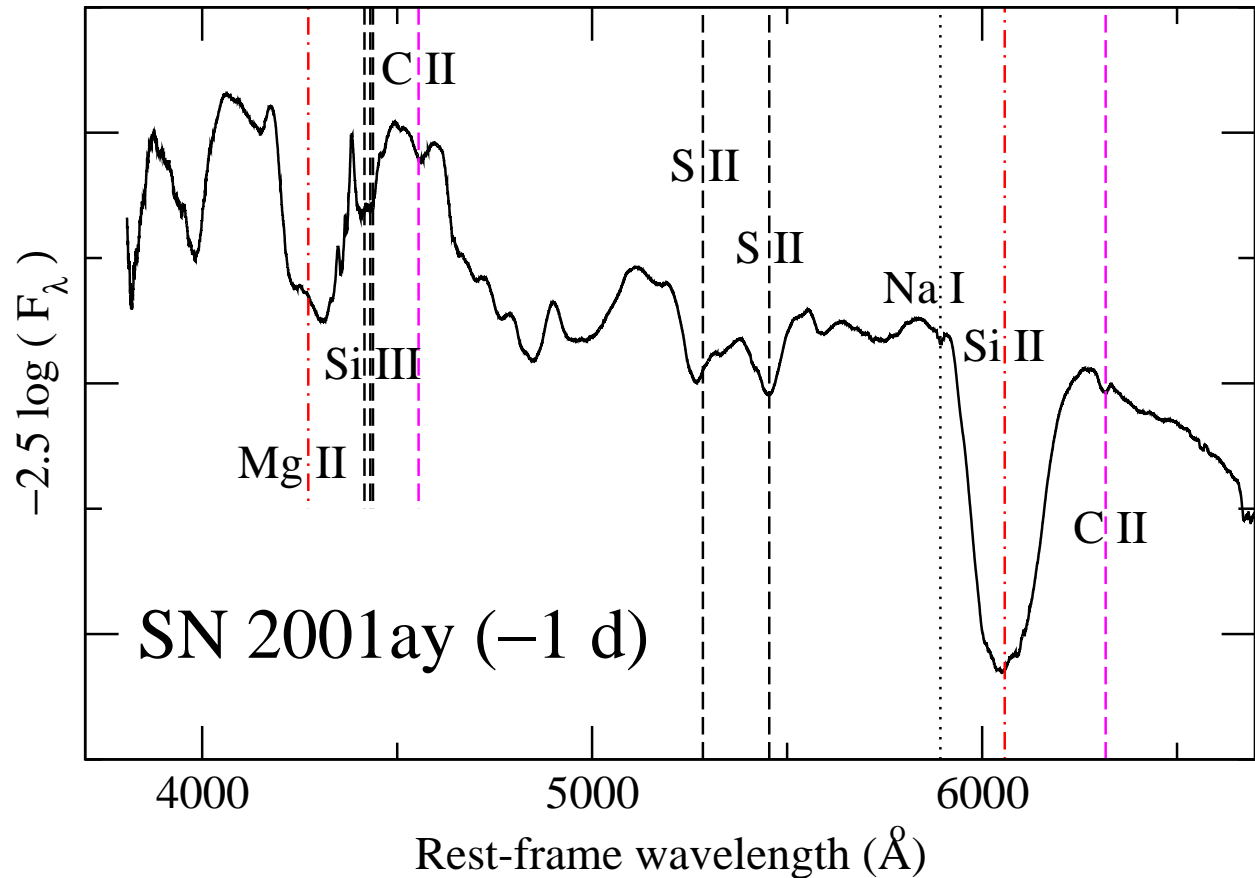
Krisciunas *et al.* Figure 11. Near-IR absolute magnitudes at maximum light of Type Ia SNe. While SNe 2001ay and 2005eq are more luminous than the average of other objects in the H band, one would not consider them significantly overluminous. The H -band point for SN 2009dc corresponds to the same epoch as in the J -band plot, but SN 2009dc brightened 0.26 mag in H over the following month. The diamond-shape points correspond to objects that peak in the near-IR later than B maximum. These objects are subluminous in all bands. See Krisciunas et al. (2009) for more details.



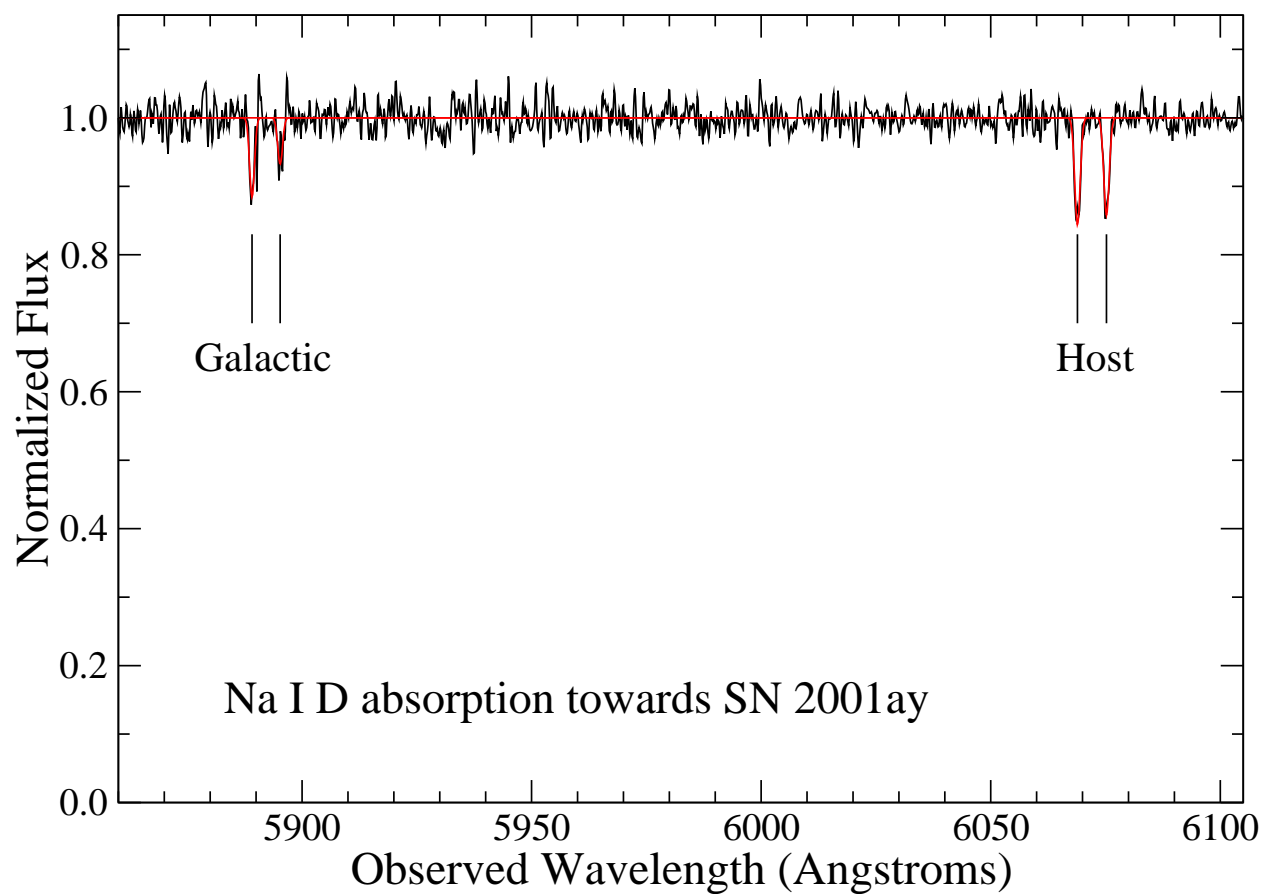
Krisciunas *et al.* Figure 12. Temporal sequence of spectra of SN 2001ay. The labels indicate the number of observer-frame days with respect to B -band maximum. Eleven which have no telescope indicated were taken with the FLWO 1.5-m. The $t = +6$ d spectrum from the KPNO 2.1-m telescope has been combined with the $t = +9$ d *HST* spectrum. The solid vertical line marks the nominal wavelength of the $\lambda_0 = 6355 \text{ \AA}$ line of Si II. The dashed vertical line shows Si II line blueshifted by $10,000 \text{ km s}^{-1}$. Telluric oxygen is identified by an Earth symbol.



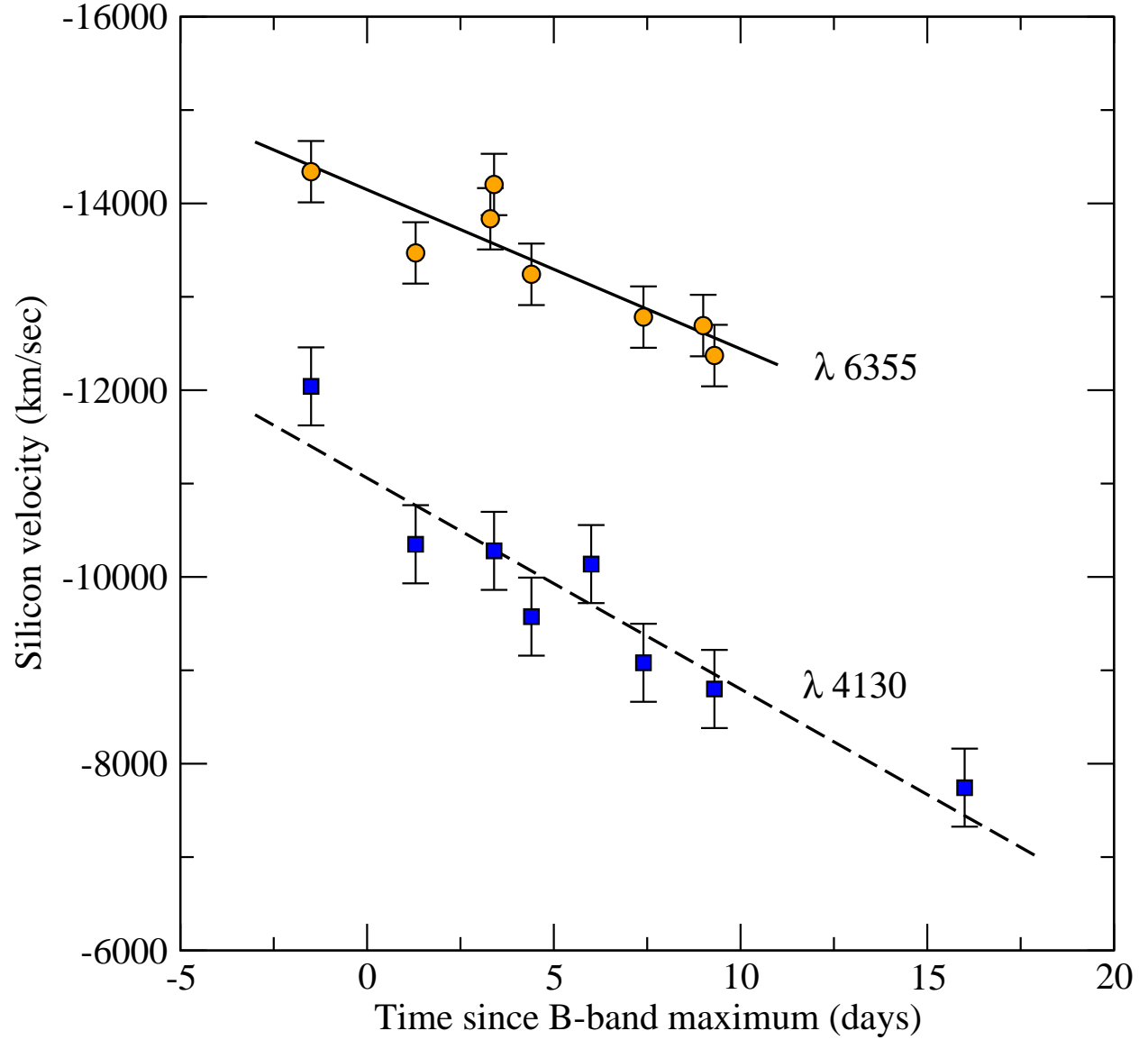
Krisciunas *et al.* Figure 13. Additional spectra of SN 2001ay obtained with the Lick Observatory 3-m Shane telescope, *HST*, and the Las Campanas Observatory 2.5-m du Pont telescope. The captioning within the figure and the meaning of the vertical lines are the same as in Figure 12. Telluric oxygen is identified by an Earth symbol.



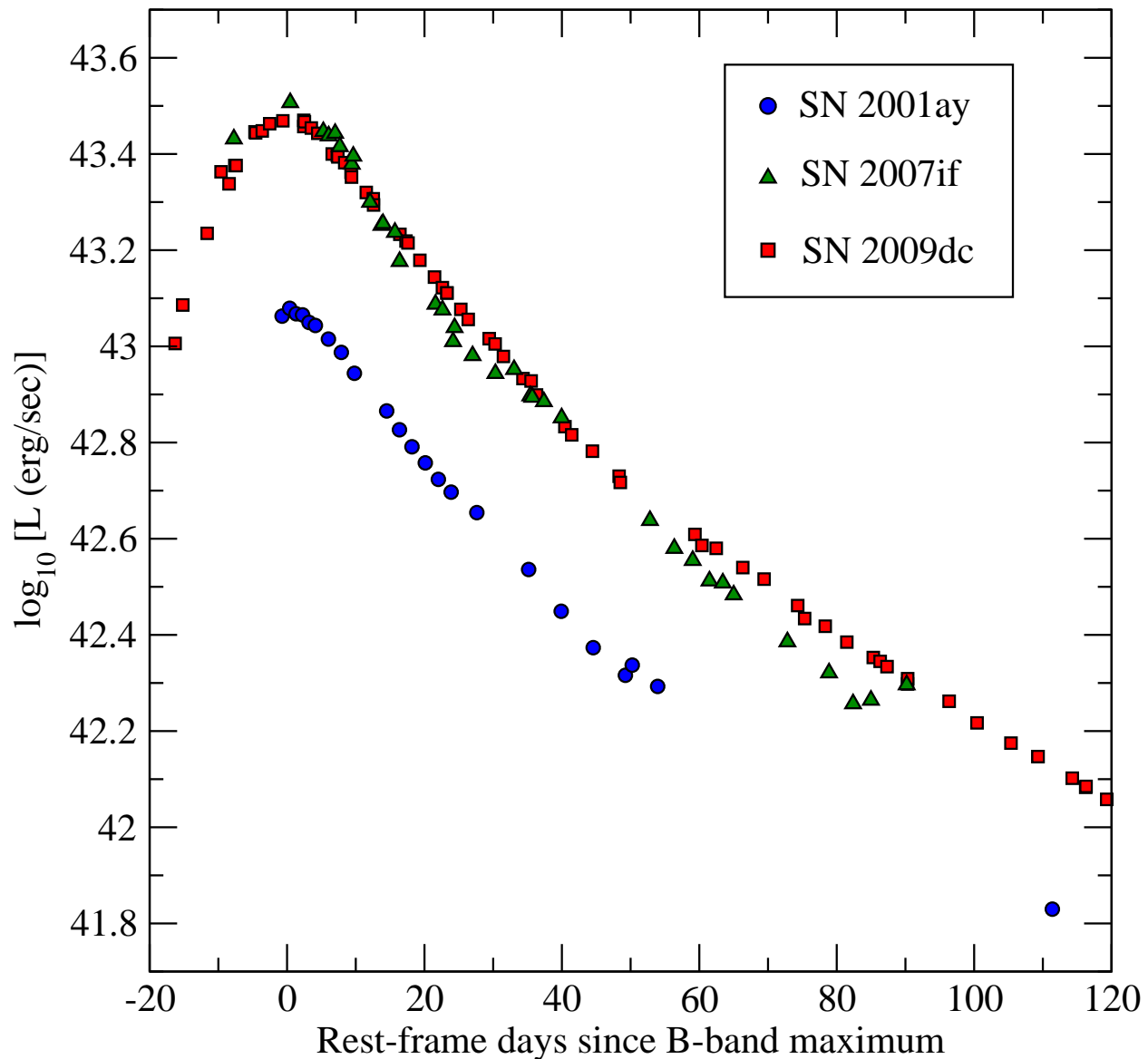
Krisciunas *et al.* Figure 14. A portion of our highest signal-to-noise ratio spectrum of SN 2001ay, taken with the Keck ESI on 2001 April 22. The dashed lines for Si III and S II correspond to blueshifts of 9000 km s^{-1} . The dashed magenta lines for C II correspond to a blueshift of $12,000 \text{ km s}^{-1}$. The dot-dashed red lines for Mg II and Si II correspond to a blueshift of $14,000 \text{ km s}^{-1}$. The dotted line for Na I is the rest wavelength.



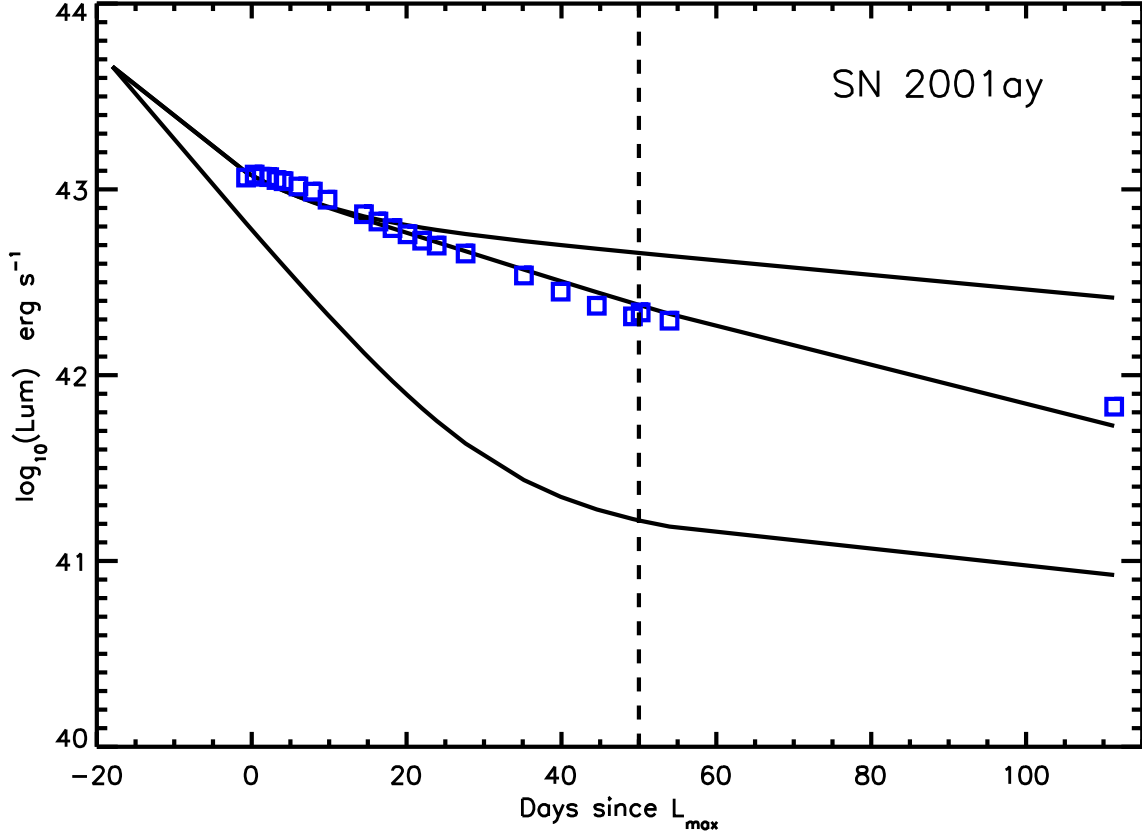
Krisciunas *et al.* Figure 15. Profile of the Na I D lines in our Keck ESI spectrum. The Milky Way and host-galaxy components are clearly present.



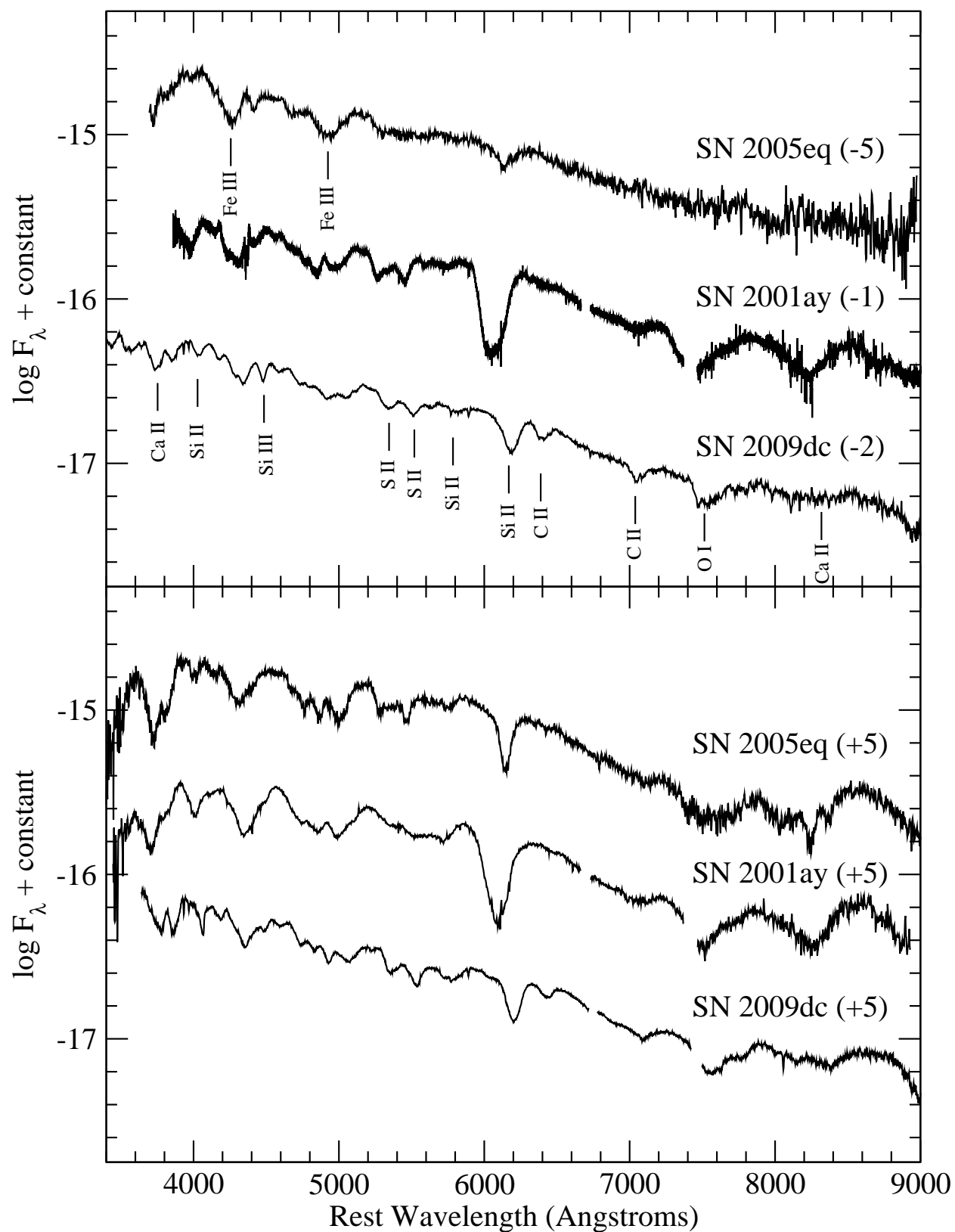
Krisciunas *et al.* Figure 16. Blueshifted velocity of two Si II lines in the spectra of SN 2001ay around maximum light. Within 1σ the gradient derived from the two lines is the same, about $200 \text{ km s}^{-1} \text{ d}^{-1}$. This qualifies SN 2001ay to be a “high velocity gradient” object (Benetti et al. 2005).



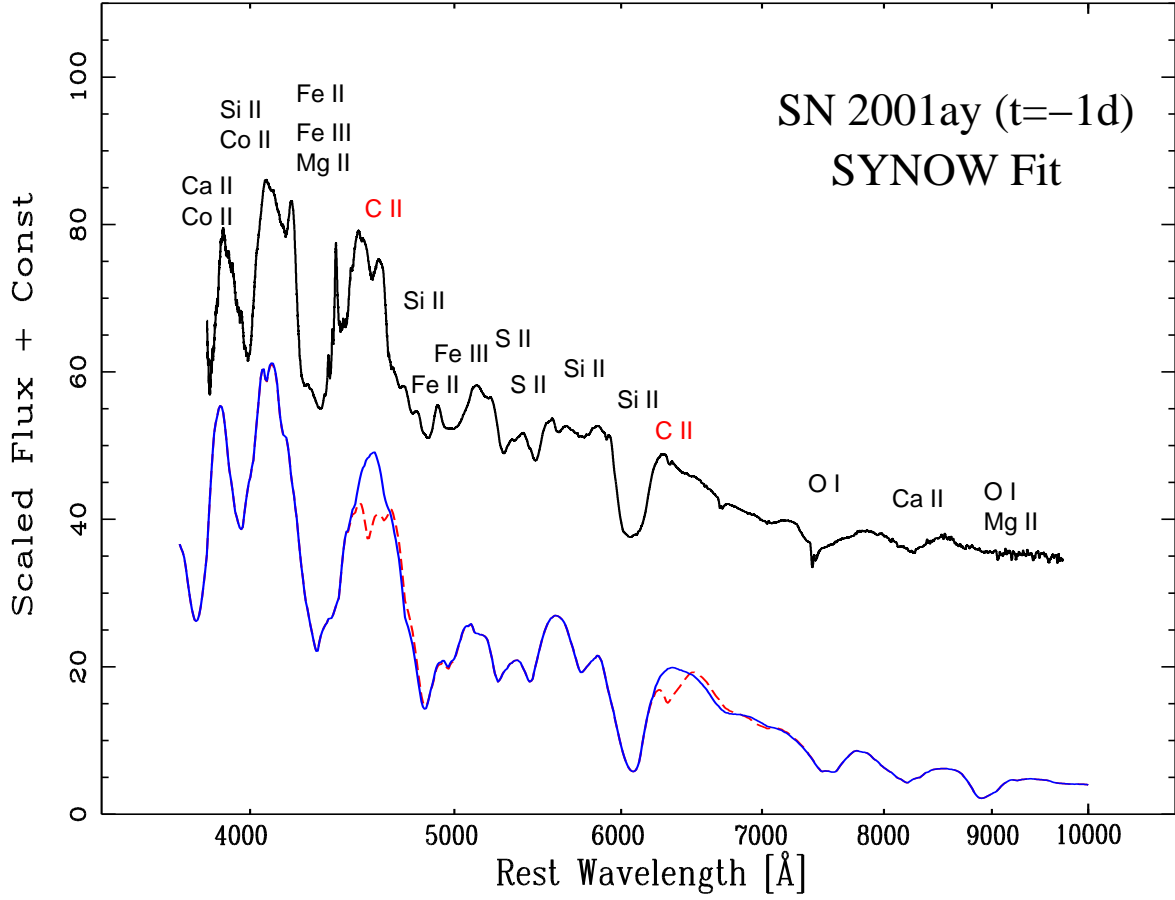
Krisciunas *et al.* Figure 17. Bolometric luminosities (L) of SNe 2001ay, 2007if (Scalzo et al. 2010), and 2009dc (Taubenberger et al. 2011), measured in erg s^{-1} . For SN 2001ay we have scaled our integrated bolometric luminosity by a factor of 1.15 to account for flux not included in our photometric bandpasses. We adopted a distance modulus of $m - M = 35.55$ mag from Table 1.



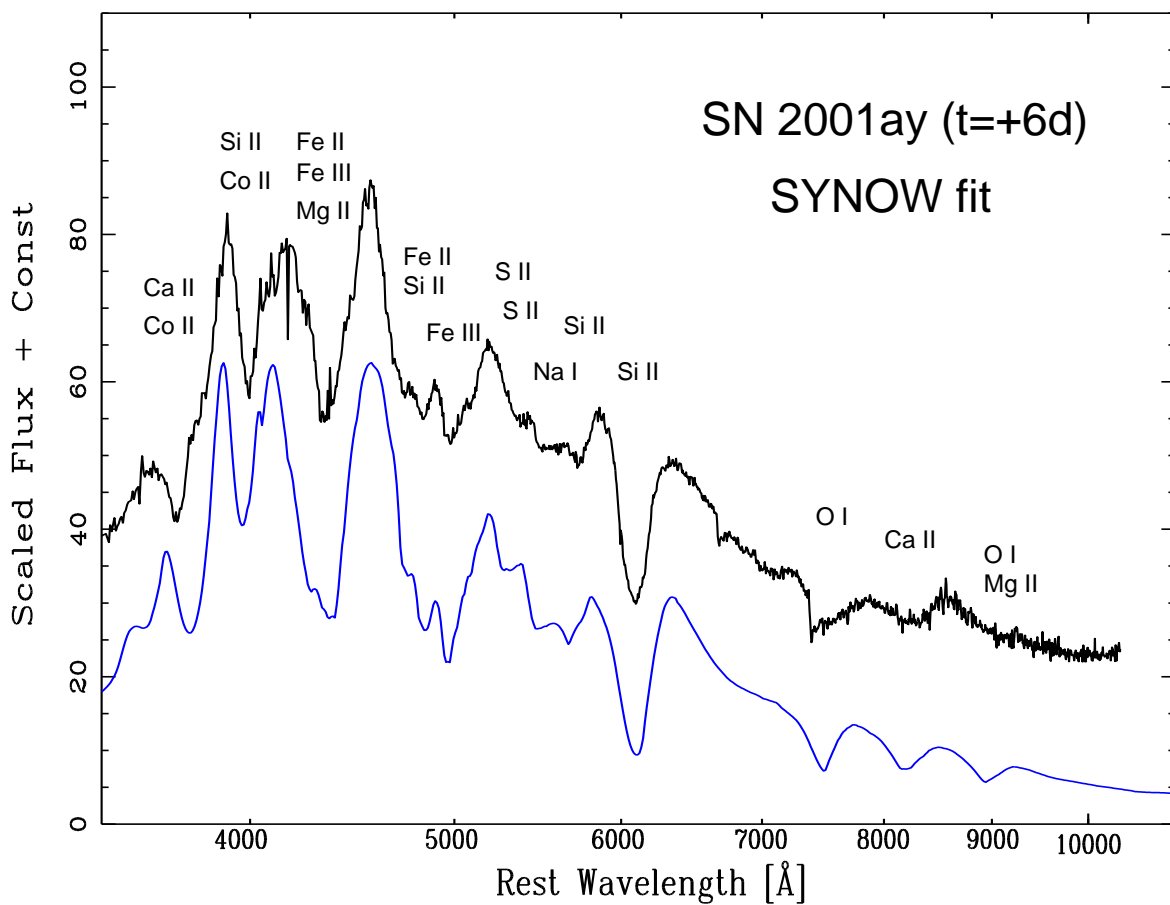
Krisciunas *et al.* Figure 18. The best-fit radioactive decay energy deposition function (middle solid line) to the UVOIR light curve (blue squares) of SN 2001ay. Here we adopt Arnett’s Rule (Arnett 1982), with $\alpha = 1.0$, which stipulates that the gamma-ray deposition matches the bolometric flux at maximum light. The top solid line corresponds to the case of complete trapping of γ rays and positrons (i.e., $\tau \gg 1$), while the bottom solid line is the case of complete γ -ray escape ($\tau \ll 1$). The vertical dashed line indicates the epoch at which the fit begins. The best fit to the latest few points suggests that the ejecta became optically thin to γ rays 57.2 ± 2.4 d past maximum brightness.



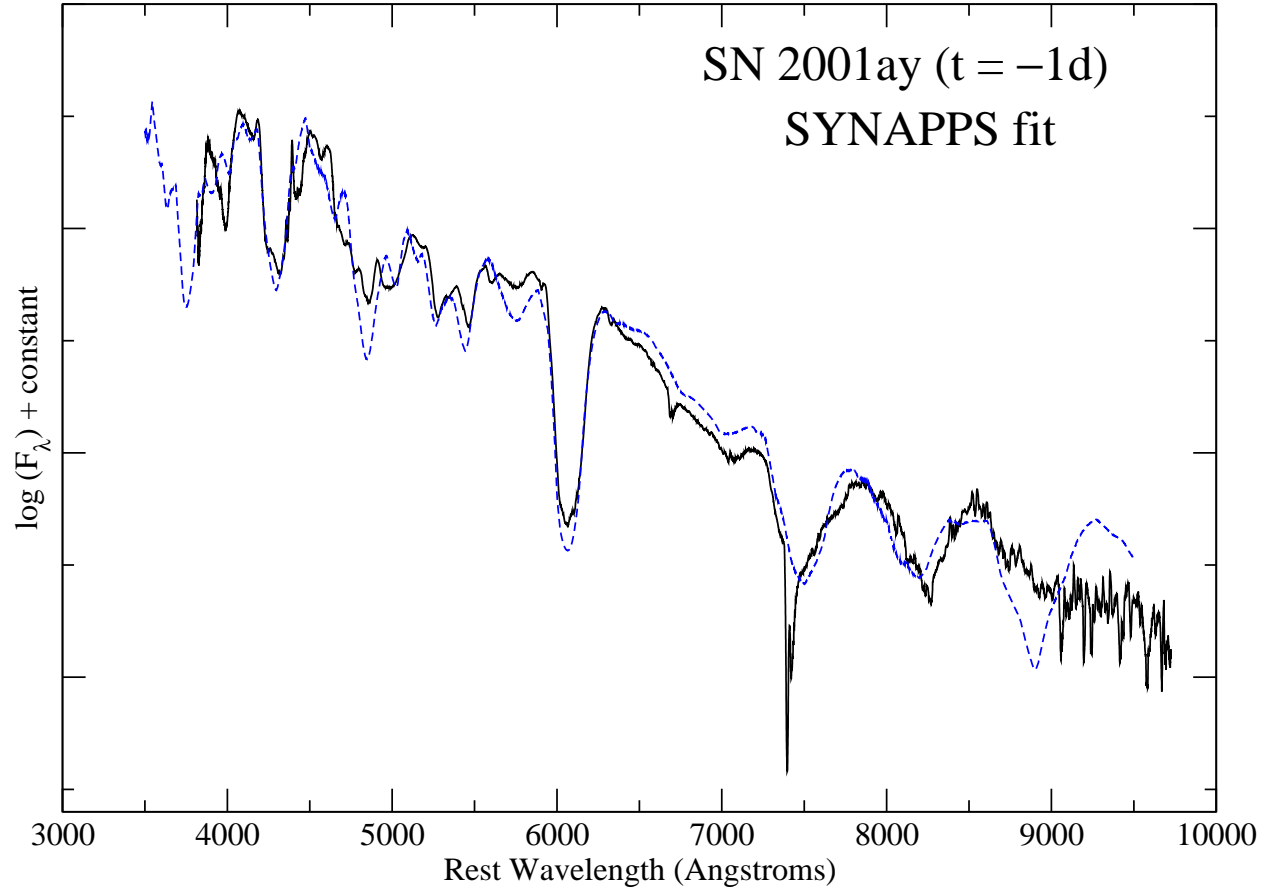
Krisciunas *et al.* Figure 19. Comparison of the optical spectra of SNe 2001ay, 2005eq, and 2009dc.



Krisciunas *et al.* Figure 20. SYNOW modeling of the optical spectrum of SN 2001ay at 1 d before *B* maximum. Upper curve = data; lower curve = SYNOW model. The dashed lines indicate the addition of C II to the model.



Krisciunas *et al.* Figure 21. SYNOW modeling of the optical spectrum of SN 2001ay 6 d after *B* maximum. Upper curve = data; lower curve = SYNOW model.



Krisciunas *et al.* Figure 22. SYNAPPS modeling of the optical spectrum of SN 2001ay 1 d before B maximum. The blue dashed line (model spectrum) can be shifted arbitrarily along the vertical axis to match the actual spectrum (shown in black).